

1                   **POMK regulates dystroglycan function via LARGE-mediated**  
2                   **elongation of matriglycan**  
3  
4

5                   **Ameya S. Walimbe<sup>1</sup>, Hidehiko Okuma<sup>1</sup>, Soumya Joseph<sup>1</sup>, Tiandi Yang<sup>1</sup>, Takahiro**  
6                   **Yonekawa<sup>1</sup>, Jeffrey M. Hord<sup>1</sup>, David Venzke<sup>1</sup>, Mary E. Anderson<sup>1</sup>, Silvia Torelli<sup>2</sup>, Adnan**  
7                   **Manzur<sup>2</sup>, Megan Devereaux<sup>1</sup>, Marco Cuellar<sup>1</sup>, Sally Prouty<sup>1</sup>, Saul Ocampo Landa<sup>1</sup>, Liping**  
8                   **Yu<sup>3</sup>, Junyu Xiao<sup>5</sup>, Jack E. Dixon<sup>6</sup>, Francesco Muntoni<sup>2, 4</sup>, and Kevin P. Campbell<sup>1\*</sup>**

9  
10                   <sup>1</sup>Howard Hughes Medical Institute, Senator Paul D. Wellstone Muscular Dystrophy Specialized  
11                   Research Center, Department of Molecular Physiology and Biophysics and Department of  
12                   Neurology, Roy J. and Lucille A. Carver College of Medicine, The University of Iowa, Iowa  
13                   City, Iowa 52242, USA

14                   <sup>2</sup>Dubowitz Neuromuscular Centre, UCL Great Ormond Street Institute of Child Health & Great  
15                   Ormond Street Hospital, London, United Kingdom.

16                   <sup>3</sup>Medical Nuclear Magnetic Resonance Facility, University of Iowa Roy J. and Lucille A. Carver  
17                   College of Medicine, B291 Carver Biomedical Research Building, 285 Newton Road, Iowa City,  
18                   IA 52242, USA

19                   <sup>4</sup>National Institute for Health Research Great Ormond Street Hospital Biomedical Research  
20                   Centre, UCL Great Ormond Street Institute of Child Health, London, United Kingdom.

21                   <sup>5</sup>The State Key Laboratory of Protein and Plant Gene Research, School of Life Sciences,  
22                   Academy for Advanced Interdisciplinary Studies, Peking-Tsinghua Center for Life Sciences,  
23                   Peking University, Beijing, 100871, China

24                   <sup>6</sup>Department of Pharmacology, Department of Cellular and Molecular Medicine, Department of  
25                   Chemistry and Biochemistry, University of California, San Diego, La Jolla, CA 92093, USA

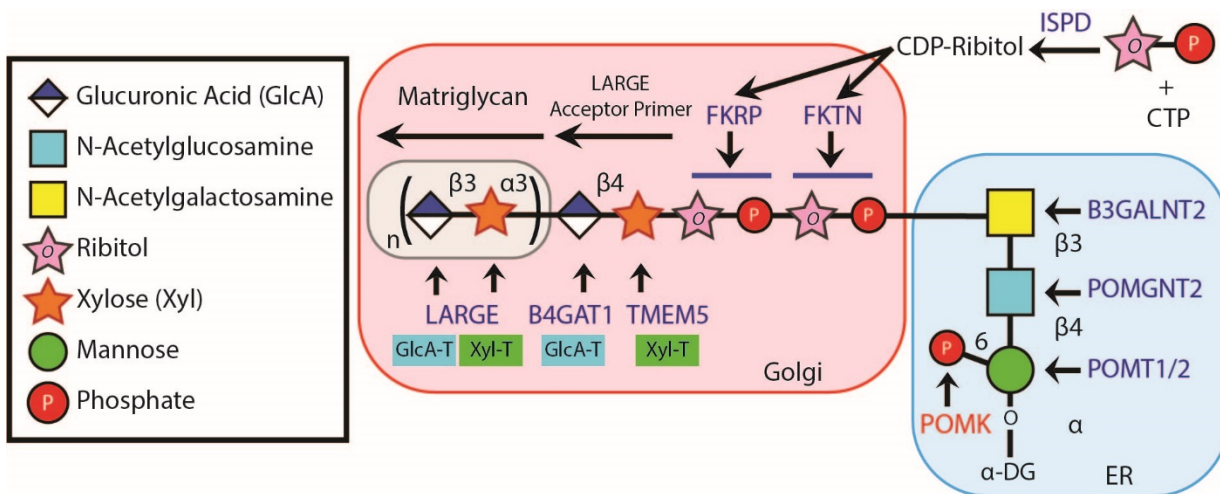
26                   \* Corresponding author

27 **Abstract**

28 Matriglycan [-GlcA- $\beta$ 1,3-Xyl- $\alpha$ 1,3-]<sub>n</sub> serves as a scaffold in many tissues for extracellular  
29 matrix proteins containing laminin-G domains including laminin, agrin, and perlecan. Like-  
30 acetylglucosaminyltransferase-1 (LARGE) synthesizes and extends matriglycan on  $\alpha$ -  
31 dystroglycan ( $\alpha$ -DG) during skeletal muscle differentiation and regeneration; however, the  
32 mechanisms which regulate matriglycan elongation are unknown. Here, we show that *Protein O-*  
33 *Mannose Kinase (POMK)*, which phosphorylates mannose of core M3 (GalNac- $\beta$ 1,3-GlcNac-  
34  $\beta$ 1,4-Man) preceding matriglycan synthesis, is required for LARGE-mediated generation of full-  
35 length matriglycan on  $\alpha$ -DG (~150 kDa). In the absence of *POMK*, LARGE synthesizes a very  
36 short matriglycan resulting in a ~90 kDa  $\alpha$ -DG in mouse skeletal muscle which binds laminin but  
37 cannot prevent eccentric contraction-induced force loss or muscle pathology. Solution NMR  
38 spectroscopy studies demonstrate that LARGE directly interacts with core M3 and binds  
39 preferentially to the phosphorylated form. Collectively, our study demonstrates that  
40 phosphorylation of core M3 by *POMK* enables LARGE to elongate matriglycan on  $\alpha$ -DG,  
41 thereby preventing muscular dystrophy.

42 **Introduction**

43 The extracellular matrix (ECM) is essential for development, regeneration and  
44 physiological function in many tissues, and abnormalities in ECM structure can lead to disease  
45 (*Rowe et al., 2008; Hudson et al., 2003*). The heteropolysaccharide [-GlcA- $\beta$ 1,3-Xyl- $\alpha$ 1,3-]<sub>n</sub>  
46 (called matriglycan) is a scaffold for ECM proteins containing laminin-G (LG) domains (e.g.  
47 laminin, agrin, and perlecan) (*Yoshida-Moriguchi et al., 2015; Hohenester, 2019; Michele et al.,*  
48 *2002; Ohtsubo et al., 2006*) and has the remarkable capacity to be tuned during skeletal muscle  
49 development and regeneration (*Goddeeris et al., 2013*). Over eighteen genes are involved in the  
50 synthesis of the post translational modification terminating in matriglycan (**Figure 1**), and defects  
51 in this process cause dystroglycanopathies, congenital and limb-girdle muscular dystrophies that  
52 can be accompanied by brain and eye defects. Like-acetylglucosaminyltransferase-1 (LARGE),  
53 synthesizes matriglycan on the cell-surface glycoprotein,  $\alpha$ -dystroglycan ( $\alpha$ -DG) (*Inamori et al.,*  
54 *2012*). Addition of matriglycan enables  $\alpha$ -DG to serve as the predominant ECM receptor in skeletal  
55 muscle and brain (*Yoshida-Moriguchi et al., 2015; Hohenester, 2019; Jae et al., 2013; Yoshida-*  
56 *Moriguchi et al., 2010; Yoshida-Moriguchi et al., 2013*). Crystal structure studies have shown  
57 that a single glucuronic acid-xylose disaccharide (GlcA-Xyl) repeat binds to laminin- $\alpha$ 2 LG4  
58 domain (*Briggs et al., 2016; Hohenester et al., 1999*), and there is a direct correlation between the  
59 number of GlcA-Xyl repeats on  $\alpha$ -DG and its binding capacity for ECM ligands (*Goddeeris et al.,*  
60 *2013; Inamori et al., 2012*). During skeletal muscle differentiation, LARGE elongates matriglycan  
61 to its full length for normal skeletal muscle function (*Goddeeris et al., 2013*). However, little is  
62 known about the mechanisms which control matriglycan elongation.

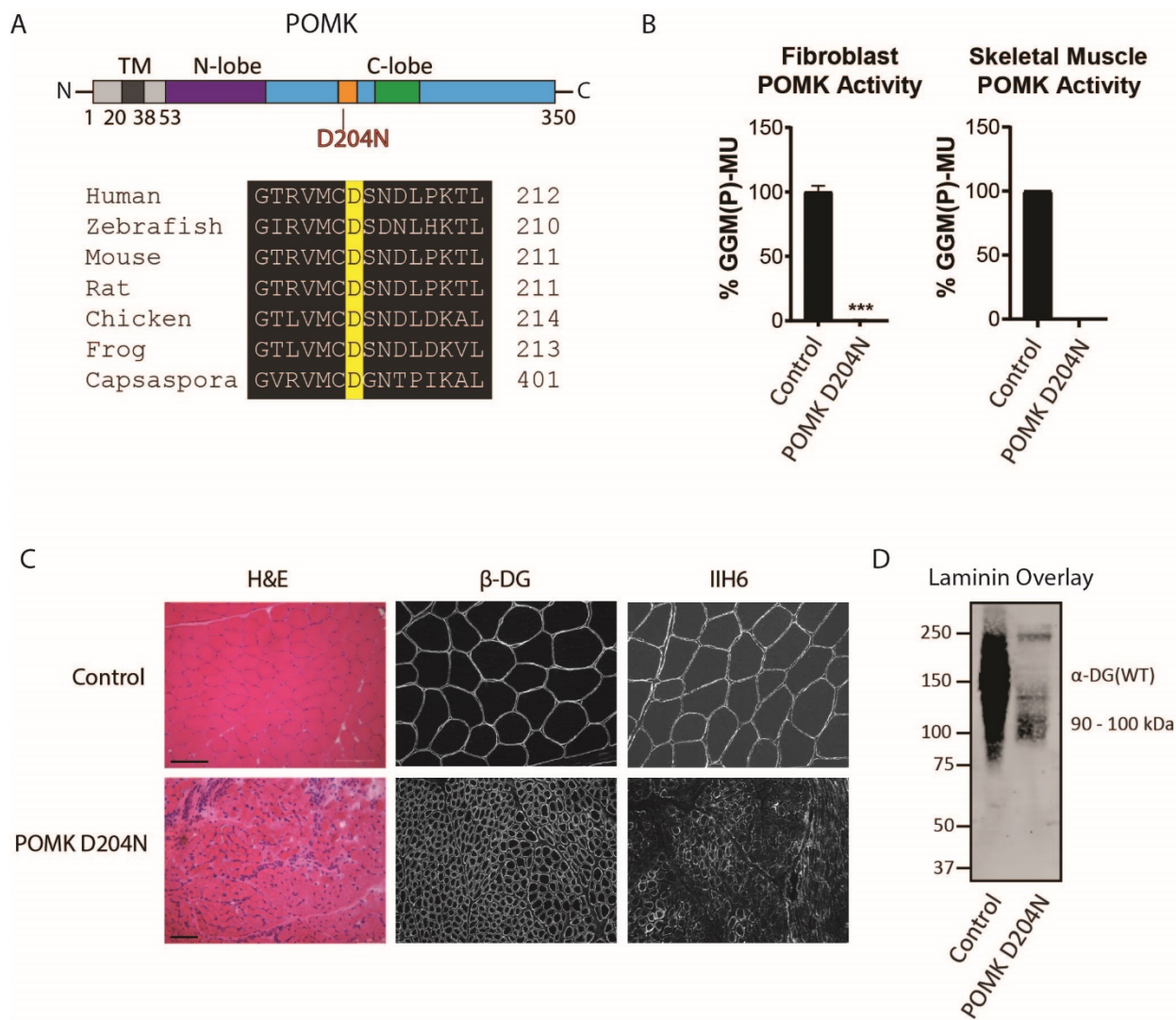


63  
64 **Figure 1.** Synthesis of the  $\alpha$ -DG Laminin-Binding Modification and Enzymes Involved.  
65 Synthesis of the laminin-binding modification begins with the addition of the core M3  
66 trisaccharide (GalNac- $\beta$ 3-GlcNac- $\beta$ 4-Man) on  $\alpha$ -DG by the sequential actions of Protein  $O$ -  
67 Mannosyltransferase-1 and 2 (POMT1/2), Protein  $O$ -linked mannose  $N$ -  
68 acetylglucosaminyltransferase 2 (POMGNT2), and  $\beta$ 1,3- $N$ -acetylgalactosaminyltransferase 2  
69 B3GALNT2, in the ER. POMK phosphorylates the C6 hydroxyl of mannose after synthesis of  
70 core M3. The phosphorylated core M3 is further elongated in the Golgi by Fukutin (FKTN),  
71 Fukutin-Related Protein (FKRP), Transmembrane Protein 5 (TMEM5),  $\beta$ 1-4-  
72 glucuronyltransferase-1 (B4GAT1), and Like-acetylglucosaminyltransferase-1 (LARGE).  
73 Isoprenoid Synthase Domain-Containing (ISPD) produces cytidine diphosphate (CDP)-Ribitol in  
74 the cytosol, and this serves as a sugar donor for the reactions catalyzed by FKTN and FKRP.  
75 LARGE synthesizes matryglycan, which directly interacts with the LG domains of matrix  
76 ligands.

77           Complete loss-of-function mutations in the dystroglycanopathy genes abrogate synthesis  
78    of the post translational modification terminating in matriglycan. Such mutations preclude addition  
79    of matriglycan and, thereby, cause the most severe form of dystroglycanopathy, Walker-Warburg  
80    Syndrome (WWS), which is lethal *in utero* or within a day or two of birth (*Yoshida-Moriguchi et*  
81    *al., 2015; Hohenester, 2019; Michele et al., 2002; Ohtsubo et al., 2006*). Protein *O*-Mannose  
82    Kinase (POMK) is a glycosylation-specific kinase that phosphorylates mannose of the core M3  
83    trisaccharide (GalNac- $\beta$ 1,3-GlcNac- $\beta$ 1,4-Man) during synthesis of the *O*-mannose-linked  
84    polysaccharide ending in matriglycan (*Yoshida-Moriguchi et al., 2015; Hohenester et al., 2019;*  
85    *Jae et al., 2013; Yoshida-Moriguchi et al., 2013; Zhu et al., 2016*). Interestingly, unlike with  
86    other dystroglycanopathy genes there are patients with complete loss-of-function mutations in  
87    POMK who suffer from mild forms of dystroglycanopathy (*Di Costanzo et al., 2014; von Renesse*  
88    *et al., 2014*), suggesting some expression of matriglycan without POMK. Here, we have used a  
89    multidisciplinary approach to show that phosphorylation of core M3 by POMK is not necessary  
90    for the LARGE-mediated synthesis of a short, non-extended form of matriglycan on  $\alpha$ -DG (~90  
91    kDa) with reduced laminin binding capacity; however, POMK is required for LARGE to generate  
92    full-length matriglycan on  $\alpha$ -DG (~150 kDa). In the absence of the phosphorylated core M3, the  
93    non-extended matriglycan on ~90 kDa  $\alpha$ -DG binds laminin and maintains specific force but cannot  
94    prevent eccentric contraction-induced force loss or skeletal muscle pathology. Furthermore,  
95    solution NMR studies demonstrated that LARGE directly interacts with core M3, binding  
96    preferentially to the phosphorylated form. Therefore, our study shows that phosphorylation of core  
97    M3 by POMK enables LARGE to elongate matriglycan on  $\alpha$ -DG. Collectively, our work  
98    demonstrates a requirement for POMK in the LARGE-mediated synthesis of full-length  
99    matriglycan and proper skeletal muscle function.

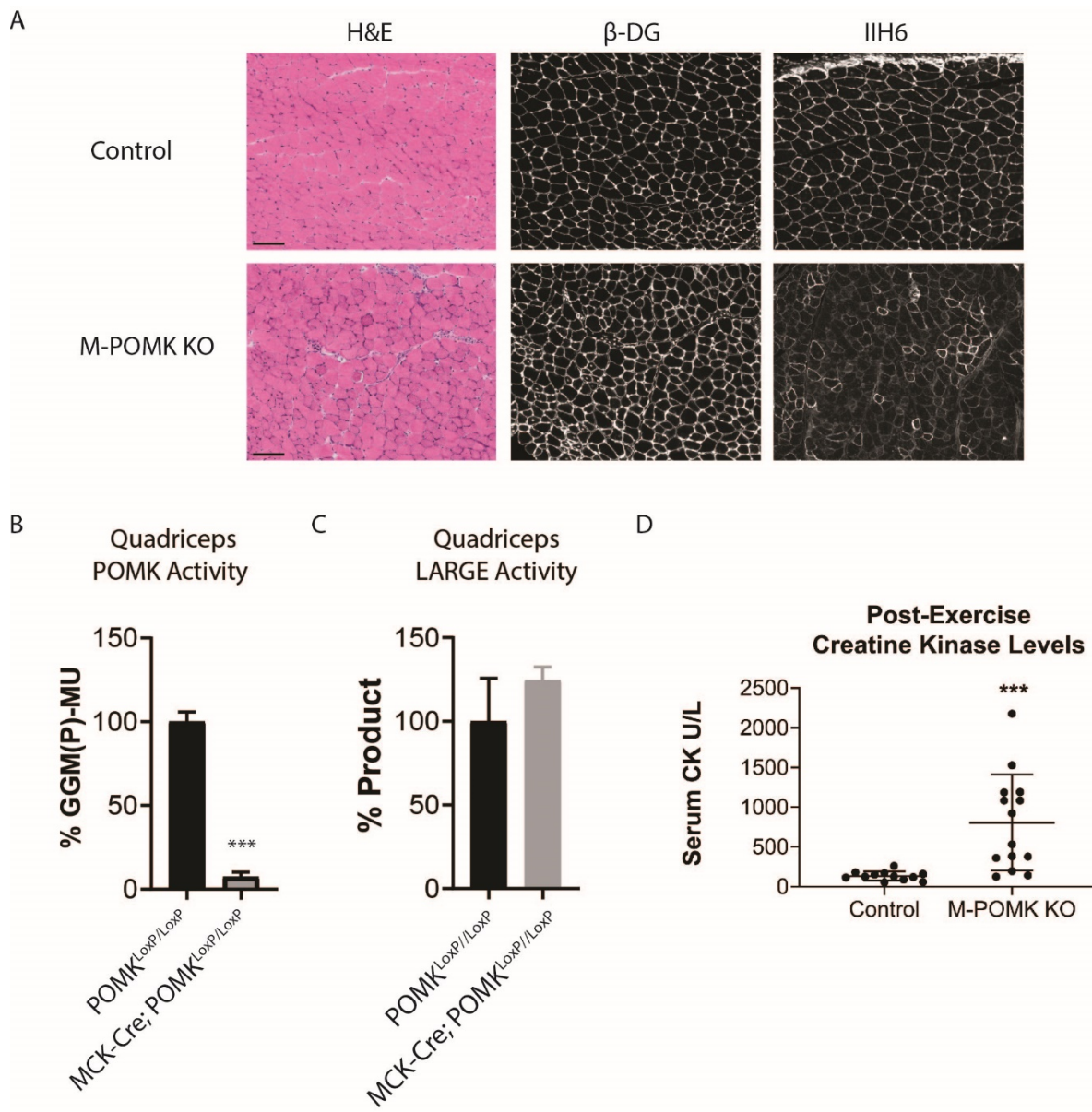
100 **Results**

101 To determine if matriglycan can be expressed in the absence of POMK function, and  
102 therefore better understand the role of POMK in matriglycan synthesis, we studied skeletal muscle  
103 from a patient (NH13-284) with a POMK (D204N) mutation (**Figure 2A**) and congenital muscular  
104 dystrophy (CMD) accompanied by structural brain malformations. D204 serves as the catalytic  
105 base in the phosphorylation reaction catalyzed by the kinase (**Figure 2A; Figure 2- Figure**  
106 **Supplement 1**) and its mutation is predicted to eliminate POMK activity (**Figure 2-Figure**  
107 **Supplement 1**) (Zhu et al., 2016). POMK activity from skin fibroblasts and skeletal muscle of  
108 patient NH13-284 (POMK D204N) was undetectable when compared to control fibroblasts and  
109 muscle, respectively (**Figure 2B**). Fibroblast LARGE activity and skeletal muscle B4GAT1  
110 activity of patient NH13-284 were similar to those of a control (**Figure 2-Figure Supplement 2A,**  
111 **2B**). Immunofluorescence analyses of POMK D204N muscle demonstrated partial  
112 immunoreactivity to IIH6 (anti-matriglycan), while the transmembrane subunit of DG,  $\beta$ -DG, was  
113 expressed normally in POMK D204N muscle (**Figure 2C**). Flow cytometry using IIH6 also  
114 demonstrated partial immunoreactivity in POMK D204N fibroblasts (**Figure 2-Figure**  
115 **Supplement 2C**). To test the effect of the POMK mutation on ligand binding we performed a  
116 laminin overlay using laminin-111. Control human skeletal muscle showed the typical broad band  
117 of  $\alpha$ -DG laminin binding centered at ~150 kDa range; in contrast, laminin binding at ~90 to 100  
118 kDa range with reduced intensity was observed in POMK D204N skeletal muscle (**Figure 2D**).



119  
120 **Figure 2.** Characterization of a Patient with a Loss-of-Function Mutation in POMK. **A**, (above)  
121 Human POMK consists of a transmembrane domain (TM) and a kinase domain (N-lobe and C-  
122 lobe). The kinase domain contains the catalytic loop (orange) and activation segment (green).  
123 (below) Alignment of protein sequences flanking the D204N mutation. The mutation alters a  
124 highly conserved aspartate that is the catalytic base of the phosphorylation reaction catalyzed by  
125 the kinase. **B**, POMK activity in control and patient NH13-284 (POMK D204N) fibroblasts (left)  
126 and skeletal muscle (right). n=3 experiments were performed in fibroblasts. Triple asterisks: p-  
127 value<0.001. Due to limited skeletal muscle, n=1 experiment was performed. **C**, Histology and  
128 immunofluorescence of control and POMK D204N skeletal muscle using IIH6 (anti-  
129 matriglycan) and a  $\beta$ -DG antibody. (Scale bars: Control- 200  $\mu$ M, POMK D204N- 75  $\mu$ M). **D**,  
130 Laminin overlay of control and POMK D204N skeletal muscle.

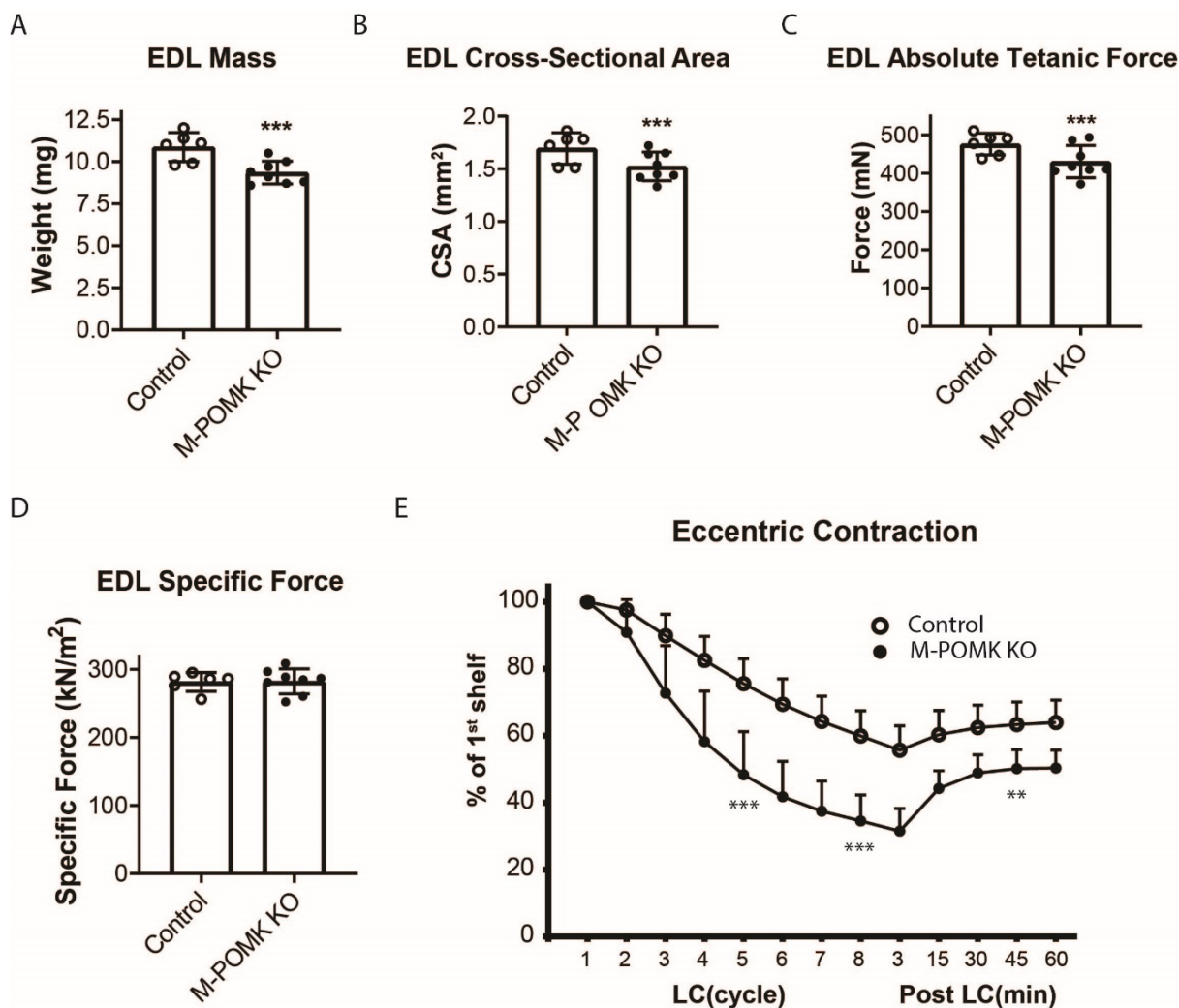
131 To understand the biochemical basis of the ~90 to 100 kDa laminin binding in the absence  
132 of POMK activity, we targeted *POMK* using LoxP sites and Cre driven by the Muscle Creatine  
133 Kinase (MCK) promoter, or both the MCK promoter and the Paired Box 7 (Pax7) promoter  
134 (**Figure 3-Figure Supplement 1, 2**) (*Brüning et al., 1998; Keller et al., 2004*) to generate muscle-  
135 specific POMK null mouse models. Histologic analyses of MCK-Cre; Pax7-Cre; POMK<sup>LoxP/LoxP</sup>  
136 (M-POMK KO) quadriceps muscles revealed hallmarks of a mild muscular dystrophy (**Figure**  
137 **3A**). Quadriceps muscle extracts of MCK-Cre; POMK<sup>LoxP/LoxP</sup> mice showed reduced POMK  
138 activity compared to POMK<sup>LoxP/LoxP</sup> muscle but had similar levels of LARGE activity (**Figure 3B**,  
139 **3C**). M-POMK KO mice also showed reductions in 2-limb grip strength and body weight and  
140 elevations in post-exercise creatine kinase (CK) levels compared to littermate control  
141 POMK<sup>LoxP/LoxP</sup> mice (**Figure 3D; Figure 3-Figure Supplement 3**). Immunofluorescence analysis  
142 of M-POMK KO muscle showed that  $\beta$ -DG is expressed at the skeletal-muscle sarcolemma  
143 (**Figure 3A**); however, like patient NH13-284 IIH6 immunoreactivity persisted in M-POMK KO  
144 muscle, but at a reduced intensity (**Figure 3A**).



145

146 **Figure 3.** Mice with a Muscle-Specific Loss of POMK Develop Hallmarks of a Mild Muscular  
147 Dystrophy. **A**, H&E and immunofluorescence analyses using IIH6 (anti-matriglycan) and an  
148 anti- $\beta$ -DG antibody of quadriceps muscles of 4-6-week-old POMK<sup>LoxP/LoxP</sup> (control) and MCK-  
149 Cre; Pax7-Cre POMK<sup>LoxP/LoxP</sup> (M-POMK KO) mice. Scale bars: 100  $\mu$ M. **B**, POMK and **C**,  
150 LARGE activity in extracts of MCK-Cre; POMK<sup>LoxP/LoxP</sup> and POMK<sup>LoxP/LoxP</sup> quadriceps skeletal  
151 muscles. Triple asterisks indicate statistical significance using a Student's unpaired t-test with a  
152 p-value<0.0001 (three replicates). **D**, Creatine kinase levels of 8-week old M-POMK KO and  
153 control mice. P-values were calculated with Student's unpaired t-test. Triple asterisks: p-value <  
154 0.05.

155 We next examined *ex vivo* force production in extensor digitorum muscles (EDL) muscles  
156 of 18-20 week-old control and M-POMK KO mice. EDL muscle mass and cross-sectional area  
157 (CSA) were reduced in M-POMK KO mice compared to control mice (**Figure 4A, 4B**).  
158 Additionally, M-POMK KO EDL absolute isometric tetanic force production was significantly  
159 lower than that of controls (**Figure 4C**). However, when normalized to muscle CSA, force  
160 production was comparable to control values (**Figure 4D**). We also sought to determine if M-  
161 POMK KO muscle could withstand repeated eccentric contractions. EDL muscles of M-POMK  
162 KO mice demonstrated greater force deficits after five and eight lengthening contractions (LC)  
163 and recovered to a lower level after 45 minutes compared to control EDL (**Figure 4E**). Together,  
164 the isometric and eccentric contractile studies suggest that the M-POMK KO EDL muscles display  
165 a specific force similar to controls (**Figure 4D**); however, muscle integrity is compromised  
166 following the stress of repeated eccentric contractions, as displayed by the slow, but progressive  
167 decline in force production and hampered recovered (**Figure 4E**). Thus, the current results  
168 demonstrate that the short matriglycan in POMK-deficient skeletal muscle can maintain specific  
169 force, but cannot prevent eccentric contraction-induced force loss or muscle pathology.



170

171 **Figure 4.** MCK-Cre; Pax7-Cre; POMK<sup>LoxP/LoxP</sup> EDL Demonstrates Eccentric Contraction-  
172 Induced Force Loss. **A**, Mass (milligrams) of POMK<sup>LoxP/LoxP</sup> (Control) and MCK-Cre; Pax7-Cre;  
173 POMK<sup>LoxP/LoxP</sup> (M-POMK KO) EDL muscles tested for force production. \*\*\*Statistical  
174 significance with Student's unpaired t-test at p-value<0.05 (p=0.0031). **B**, Cross-sectional area  
175 (CSA) of EDL muscles. \*\*\*Statistical significance using Student's unpaired t-test with p-  
176 value<0.05 (p=0.0463). **C**, Maximum Absolute Tetanic Force production by Control and M-  
177 POMK KO EDL muscles. \*\*\*Statistical significance using Student's unpaired t-test with a p-  
178 value<0.05 (p=0.0395). **D**, Specific Force Production in Control and M-POMK KO extensor  
179 digitorum longus (EDL) muscles. (p=0.921). **E**, Force deficit and force recovery in  
180 POMK<sup>LoxP/LoxP</sup> (Control, n=3 mice) and (M-POMK KO, n=4 mice) mice after eccentric  
181 contractions. Individual extensor digitorum longus (EDL) muscles from 18-20-week-old male  
182 mice were tested and are represented by open (Control) or closed (M-POMK KO) circles.  
183 \*\*\*Statistical significance using Student's unpaired t-test with a p-value<0.001 compared to  
184 Control EDL at given LC cycle. \*\*Statistical significance using Student's unpaired t-test with a  
185 p-value=0.0027 compared to Control EDL at given LC cycle. Error bars represent SD.

186 Biochemical analysis of control and M-POMK KO muscle showed a typical, lower  
187 molecular weight (MW)  $\alpha$ -DG with anti-core DG antibody (**Figure 5A**), however, on laminin  
188 overlay, we observed laminin binding at 90-100 kDa (**Figure 5B**), similar to POMK D204N  
189 skeletal muscle (**Figure 2D**). IIH6 also showed binding at 90-100 kDa (**Figure 5C**). Solid-phase  
190 binding analyses of M-POMK KO and MCK-Cre; POMK<sup>LoxP/LoxP</sup> skeletal muscle demonstrated a  
191 reduced binding capacity (relative  $B_{max}$ ) for laminin-111 compared to control muscle (**Figure 5-**  
192 **Figure Supplement 1A**), but higher than that of *LARGE*<sup>myd</sup> muscle, which lacks matriglycan due  
193 to a deletion in *LARGE*.

194 To determine if matriglycan is responsible for the laminin binding at 90-100 kDa in  
195 POMK-null muscle, we treated glycoproteins enriched from skeletal muscles of M-POMK KO  
196 and MCK-Cre; POMK<sup>LoxP/LoxP</sup> mice with two exoglycosidases,  $\alpha$ -Xylosidase and  $\beta$ -  
197 Glucuronidase, which in combination digest matriglycan (**Figure 5-Figure Supplement 1B, 2A,**  
198 **2B**) (**Briggs et al., 2016**). Laminin overlay and solid phase analysis showed a reduction in laminin  
199 binding from these muscles after dual exoglycosidase digestion (**Figure 5D, 5E; Figure 5- Figure**  
200 **Supplement 2A, 2B**).

201

202

203

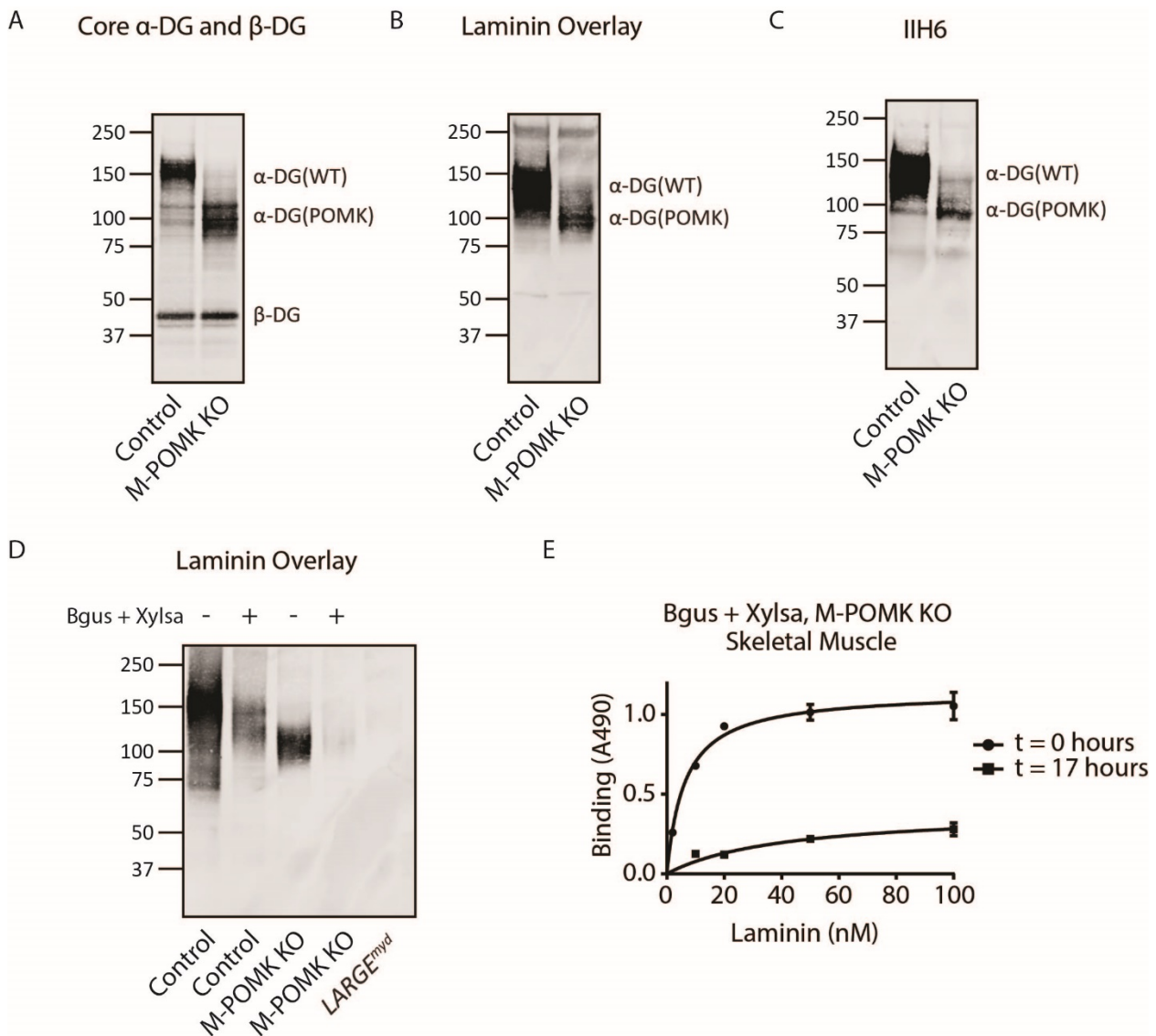
204

205

206

207

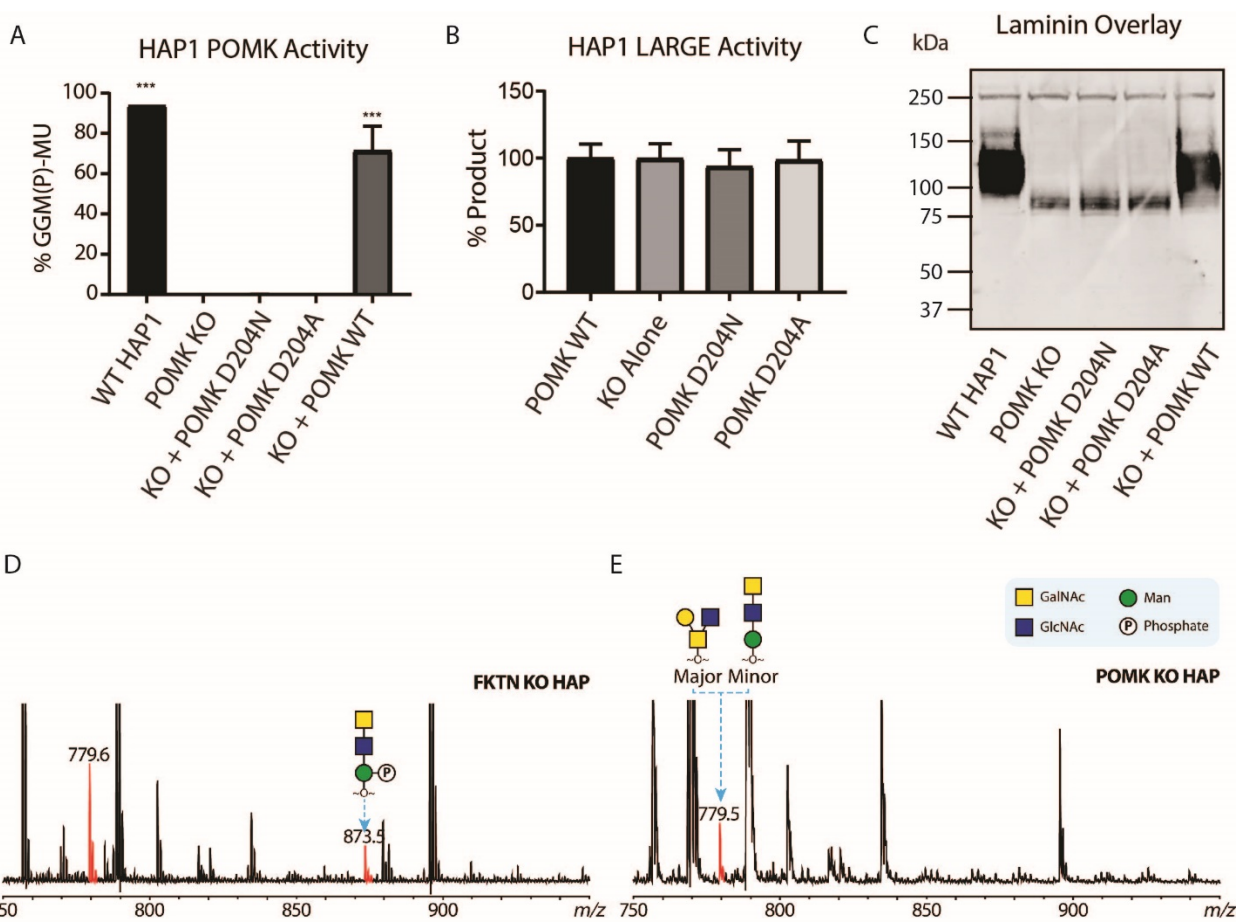
208



209

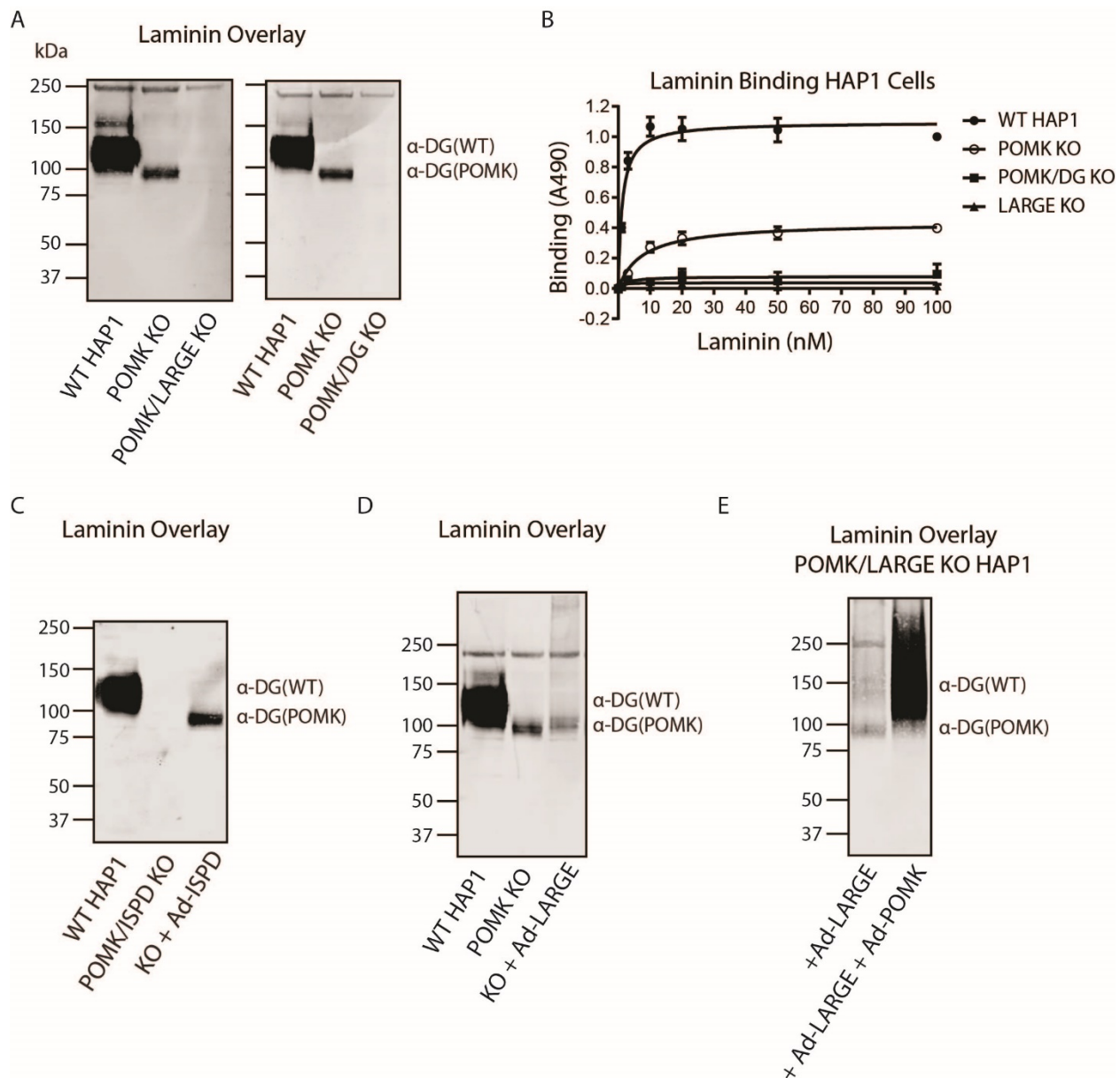
210 **Figure 5.** Mice with a Muscle-Specific Loss of POMK Express Matriglycan. **A**, Biochemical  
211 analysis of Control and M-POMK KO skeletal muscle. Glycoproteins were enriched from  
212 quadriceps skeletal muscles of mice using wheat-germ agglutinin (WGA)-agarose.  
213 Immunoblotting was performed with antibody AF6868, which recognizes core  $\alpha$ -DG and  $\beta$ -DG  
214 (three replicates). **B**, Laminin overlay of quadriceps muscles of Control and M-POMK KO mice  
215 (three replicates). **C**, IIH6 immunoblotting of Control and M-POMK KO quadriceps muscle.  
216 **D, E**, Laminin overlay (**D**) and Solid phase analysis (**E**) of skeletal muscles of M-POMK KO  
217 mice treated in combination with two exoglycosidases,  $\alpha$ -xylosidase (Xylsa) and  $\beta$ -glucuronidase  
218 (Bgus) for 17 hours (three replicates).

219 To study the role of POMK further, we used *POMK* KO HAP1 cells, which have  
220 undetectable levels of POMK activity and expression (**Figure 6A; Figure 6- Figure Supplement**  
221 **1A**) (Zhu et al., 2016). A mass spectrometry (MS)-based glycomic analysis of *O*-glycans carried  
222 by recombinantly-expressed DG mucin-like domain indicated the absence of an MS peak at *m/z*  
223 873.5 corresponding to phosphorylated core M3 *O*-glycan (**Figure 6D, 6E**), consistent with an  
224 undetectable level of POMK activity in *POMK* KO HAP1 cells. Compared to WT HAP1 cells,  
225 immunoblots of *POMK* KO HAP1 cells showed a reduction in IIH6 immunoreactivity, a decrease  
226 in MW of core  $\alpha$ -DG, and the presence of laminin binding at ~90 kDa on laminin overlay (**Figure**  
227 **6C; Figure 6-Figure Supplement 1B, 1C**). Laminin binding on overlay was rescued only after  
228 adenoviral transduction with wild-type (WT) POMK (POMK WT), but not with POMK containing  
229 D204N (POMK D204N) or D204A (POMK D204A) mutations (**Figure 6C**). POMK D204N also  
230 lacked POMK activity *in vitro* but showed normal B4GAT1, B3GALNT2, and LARGE activity,  
231 thus confirming the pathogenicity of the D204N mutation (**Figure 6A, 6B; Figure 6- Figure**  
232 **Supplement 1D, 1E**).



234 **Figure 6. POMK D204N lacks Catalytic Activity.** **A**, POMK or **B**, LARGE activity in *POMK*  
235 KO HAP1 cells transduced with adenoviruses encoding POMK D204N, D204A, or POMK WT.  
236 Asterisks: P-value<0.001 compared to *POMK* KO alone using One-Way ANOVA with  
237 Dunnett's Test for Multiple Comparisons (three replicates). **C**, Laminin overlay of *POMK* KO  
238 HAP1 cells expressing the indicated POMK mutants. **D**, **E**, Mass Spectrometry (MS)-based *O*-  
239 glycomic analyses of DG mucin-like domain (DG390TevHis) expressed in *Fukutin* (*FKTN*) (**D**)  
240 or *POMK* (**E**) KO HAP1 cells. *O*-glycans were released from the protein backbone and  
241 permethylated prior to Matrix-Assisted Laser Desorption/Ionization time-of-flight (MALDI-  
242 TOF) analyses. MS peaks at *m/z* 779.5 (779.6) correspond to a mixture of core 2 and core M3 *O*-  
243 glycan, and at 873.5, phosphorylated core M3 *O*-glycan (red).

244 To directly test if LARGE is required for synthesis of the 90 kDa laminin-binding  
245 glycoprotein in *POMK* KO HAP1 cells, we studied *POMK/LARGE* KO HAP1 cells, which bear a  
246 CRISPR/Cas9-mediated deletion in *LARGE* as well as *POMK*. *POMK/LARGE* KO HAP1 cells  
247 demonstrated the absence of the laminin binding at 90 kDa (**Figure 7A**; **Figure 7-Figure**  
248 **Supplement 1A, 1B**), indicating that LARGE is required for the synthesis of the matriglycan  
249 responsible for laminin binding at 90 kDa. Moreover, *POMK/DG* KO HAP1 cells demonstrated a  
250 complete absence of laminin binding (**Figure 7A**) and IIH6 immunoreactivity at 90 kDa (**Figure**  
251 **7- Figure Supplement 1C**), demonstrating that  $\alpha$ -DG is the glycoprotein that binds laminin in the  
252 absence of POMK. We, therefore, refer to this glycoprotein as POMK-null  $\alpha$ -DG ( $\alpha$ -DG(POMK)).  
253 Since the length of matriglycan correlates with its binding capacity for ECM ligands (*Goddeeris*  
254 *et al.*, 2013), we hypothesized that, given the MW of  $\alpha$ -DG(POMK) at 90 kDa, the glycan must be  
255 shorter than full-length matriglycan, and therefore, have a lower  $B_{max}$  for laminin. We measured  
256 the binding capacity of HAP1  $\alpha$ -DG using solid-phase binding assays.  $B_{max}$  of  $\alpha$ -DG(POMK) for  
257 laminin-111 was reduced compared to wild-type  $\alpha$ -DG ( $\alpha$ -DG(WT)) but was greater than that of  
258  $\alpha$ -DG from *LARGE* KO HAP1 cells (**Figure 7B**). *POMK/DG* KO HAP1 cells showed a reduction  
259 in  $B_{max}$  compared to *POMK* KO HAP1 cells, but similar to the low levels observed in *LARGE* KO  
260 HAP1 cells (**Figure 7B**). These data indicate that a short, non-extended form of matriglycan is  
261 synthesized on  $\alpha$ -DG(POMK), and this short form has a lower binding capacity for laminin-111,  
262 thus exhibiting a reduced level of  $\alpha$ -DG receptor function.

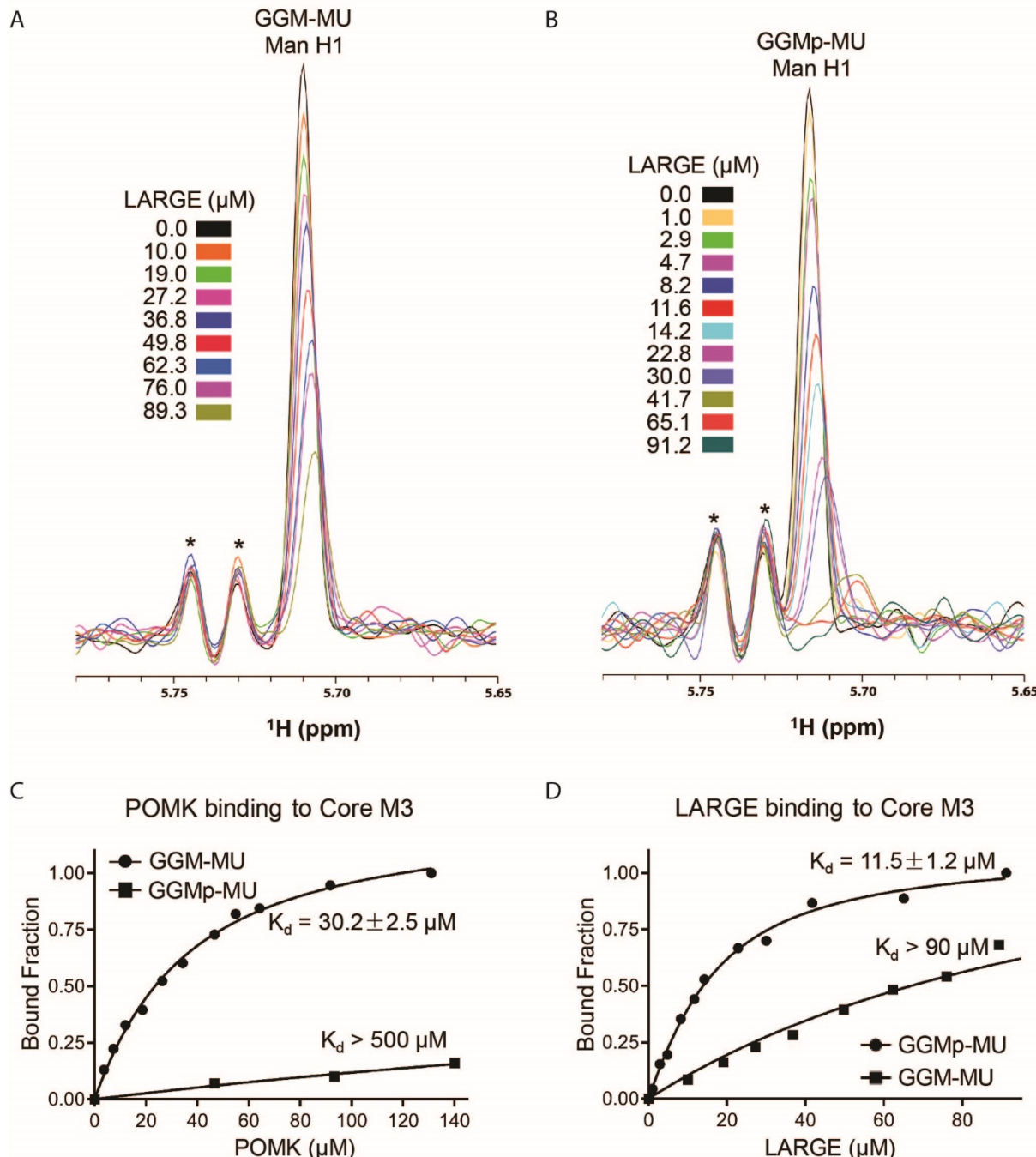


270 After POMK phosphorylates core M3, Fukutin (FKTN) modifies GalNac with ribitol-  
271 phosphate for synthesis of full-length matriglycan (**Figure 1**) (*Yoshida-Moriguchi et al., 2015;*  
272 *Hohenester, 2019; Kanagawa et al., 2016*). Overexpression in *POMK* KO HAP1 cells of  
273 Isoprenoid Synthase Domain-Containing (ISPD), which synthesizes the substrate (CDP-ribitol) of  
274 FKTN (**Figure 1**), increases the amount of matriglycan (without changing its MW) responsible for  
275 laminin binding at 90 kDa (**Figure 7-Figure Supplement 2A, 2B, 2C**) (*Willer et al., 2012; Gerin*  
276 *et al., 2016; Riemersma et al., 2015*). HAP1 cells lacking both POMK and ISPD do not express  
277 matriglycan, and adenoviral transduction of these cells with *ISPD* restores the 90 kDa laminin  
278 binding (**Figure 7C; Figure 7- Figure Supplement 2D, 2E**). FKTN overexpression in *POMK* KO  
279 HAP1 cells also increased the 90 kDa laminin binding (**Figure 7- Figure Supplement 3A, 3B,**  
280 **3C**). These experiments collectively support a requirement for CDP-ribitol for synthesis of the  
281 non-extended form of matriglycan. This synthesis also requires the N-terminal domain of  $\alpha$ -DG  
282 (DGN) (*Hara et al., 2011; Kanagawa et al., 2004*), as a DG mutant lacking the DGN (DGE)  
283 expressed in *POMK/DG* KO HAP1 cells did not show laminin binding at 90 kDa (**Figure 7-Figure**  
284 **Supplement 4A, 4B, 4C**). Similar experiments also indicated that synthesis of the non-extended  
285 matriglycan in HAP1 cells requires threonine-317 of the mucin-like domain of  $\alpha$ -DG (**Figure 7-**  
286 **Figure Supplement 4A, 4B, 4C**).

287 Overexpression of LARGE can rescue the defect in matriglycan synthesis in distinct forms  
288 of CMD as well as in *LARGE* KO HAP1 cells by generating very high molecular weight  
289 matriglycan (**Figure 7-Figure Supplement 5A**) (*Barresi et al., 2004*). However, overexpression  
290 of LARGE in *POMK* or *POMK/LARGE* KO HAP1 cells did not produce very high molecular  
291 weight matriglycan (**Figure 7D, 7E; Figure 7- Figure Supplement 5B, 5C, 5D**). Only the rescue  
292 of *POMK/LARGE* KO HAP1 cells with POMK enabled LARGE to synthesize high molecular

293 weight matriglycan (**Figure 7E; Figure 7- Figure Supplement 5D**). These findings indicate that  
294 LARGE requires phosphorylated core M3 to extend matriglycan on  $\alpha$ -DG to its mature and high  
295 molecular weight forms.

296 To understand why phosphorylated core M3 is needed for LARGE to elongate matriglycan,  
297 we measured the binding affinity of LARGE, as well as POMK, for the phosphorylated core M3  
298 using solution NMR. We previously showed that the unphosphorylated core M3 binds to POMK  
299 with high affinity (*Zhu et al., 2016*). The mannose anomeric proton (Man H1) is well resolved and  
300 its intensity decreases only slightly with increasing POMK protein concentration (**Figure 8-**  
301 **Figure Supplement 1A**). By fitting the intensity changes of the Man H1 peak as a function of  
302 POMK concentration, we obtained a dissociation constant of  $> 500 \mu\text{M}$  (**Figure 8C; Figure 8-**  
303 **Figure Supplement 1A, 1B**). These results indicate that, compared to the unphosphorylated core  
304 M3 of GGM-MU, the phosphorylated core M3 of GGMP-MU binds to POMK with a much weaker  
305 affinity. Then, we measured the binding affinities of LARGE for GGMP-MU and GGM-MU in a  
306 similar manner. Our results showed that LARGE binds with greater affinity to GGMP-MU  
307 compared to GGM-MU ( $K_d = 11.5 \pm 1.2 \mu\text{M}$  for GGMP-MU compared to  $K_d > 90 \mu\text{M}$  for GGM-  
308 MU) (**Figure 8A, 8B, 8D**). This indicates that the core M3 phosphate increases the binding affinity  
309 of LARGE for core M3 and could explain the ability of LARGE to elongate matriglycan in the  
310 presence of POMK.



311 **Figure 8.** NMR Analyses of POMK and LARGE Binding to GGM-MU and GGMP-MU. **A, B,**  
312 1D  $^1\text{H}$  NMR spectra of the anomeric region of GGM-MU and GGMP-MU, respectively, were  
313 acquired for the glycan concentration of 10.0  $\mu\text{M}$  in the presence of various concentrations of  
314 LARGE as indicated. The peak Man H1 is derived from the mannose anomeric H1 proton. Stars  
315 indicate impurity peaks derived from buffer. **C, D,** Fitting of the NMR binding data of POMK  
316 (C) and LARGE (D) to core M3 glycans of GGM-MU and GGMP-MU, respectively. The bound  
317 fraction was obtained from the NMR titration data by measuring the difference in the peak  
318 intensity of the anomeric proton Man H1 in the absence (free form) and presence (bound form)  
319 of POMK or LARGE, then divided by the peak intensity of the free form.

320 **Discussion**

321 POMK is a novel muscular dystrophy gene that phosphorylates mannose of the core M3  
322 trisaccharide (GalNac- $\beta$ 1,3-GlcNac- $\beta$ 1,4-Man) on  $\alpha$ -DG during synthesis of the *O*-mannose-  
323 linked polysaccharide ending in matriglycan. LARGE is responsible for the synthesis of  
324 matriglycan, and addition of matriglycan enables  $\alpha$ -DG to serve as a predominant ECM receptor  
325 in many tissues, in particular, skeletal muscle and brain. Over eighteen genes are implicated in  
326 matriglycan synthesis, and complete loss-of-function mutations in these genes abrogate synthesis  
327 of the *O*-mannose linked modification and preclude the addition of matriglycan, thereby leading  
328 to dystroglycanopathies, congenital and limb-girdle muscular dystrophies with or without  
329 structural brain and eye abnormalities. Here, we have used a multidisciplinary approach to show  
330 that the absence of POMK activity does not preclude addition of matriglycan. Instead, in the  
331 absence of core M3 phosphorylation by POMK, LARGE synthesizes a very short, non-extended  
332 form of matriglycan on  $\alpha$ -DG (~90 kDa); however, in order to generate full-length mature  
333 matriglycan on  $\alpha$ -DG (~150 kDa), LARGE requires phosphorylation of core M3 by POMK  
334 (**Figure 8- Figure Supplement 2A, 2B**).

335 Our study shows that the short form of matriglycan is able to bind to laminin with high  
336 affinity and thus enables  $\alpha$ -DG (POMK) to function as an ECM receptor. Given the very small  
337 increase in apparent MW in  $\alpha$ -DG(POMK) compared to  $\alpha$ -DG from cells and muscle lacking  
338 LARGE (**Figure 5-Figure Supplement 2A; Figure 7-Figure Supplement 1A; Figure 8-Figure**  
339 **Supplement 3A**), the short, non-extended form of matriglycan likely contains very few Xyl-GlcA  
340 repeats. However, it can still bind laminin since only a single Xyl-GlcA repeat is needed for  
341 laminin binding (**Briggs et al., 2016**) but it cannot function as an ECM scaffold. This short  
342 matriglycan likely attenuates muscular dystrophy in our patient with a complete loss-of-function

343 mutation in POMK, preventing the severe CMD phenotype that is observed in the complete  
344 absence of the other known dystroglycanopathy genes.

345 Muscle-specific POMK KO mice express the short, non-extended form of matriglycan on  
346 ~90 kDa  $\alpha$ -DG and develop a mild muscular dystrophy phenotype. Muscle physiology studies  
347 demonstrate that the short matriglycan expressed in the absence of POMK can maintain specific  
348 force but cannot prevent eccentric contraction-induced force loss or skeletal muscle pathology.  
349 Interestingly, missense mutations in FKRP that cause LGMD2I also show reduced expression of  
350 matriglycan (*Yoshida-Moriguchi et al., 2015*) and exhibit a milder muscular dystrophy. Thus, M-  
351 POMK KO mice are an excellent model of milder forms of dystroglycanopathy in which short  
352 matriglycan is expressed and will be useful for future studies of these forms of dystroglycanopathy.

353 Biochemical studies using various POMK null HAP1 cell lines demonstrated that the  
354 synthesis of the short, non-extended form of matriglycan, like full-length matriglycan, requires  
355 LARGE, DGN, CDP-ribitol and threonine-317 of the mucin-like domain of  $\alpha$ -DG. LARGE is  
356 known to interact with DGN, and this interaction is required for LARGE to modify  $\alpha$ -DG during  
357 synthesis of full-length matriglycan (*Kanagawa et al., 2004; Hara et al., 2011*). Cell biological  
358 experiments demonstrated that LARGE can act on  $\alpha$ -DG in the absence of the phosphorylated  
359 core M3 but requires DGN. The binding of LARGE to the DGN likely enables LARGE to  
360 generate the non-extended matriglycan on an acceptor oligosaccharide lacking phosphorylated  
361 core M3. Indeed, that threonine-317, closest to the DGN, is modified with the non-extended form  
362 of matriglycan further indicates the importance of the DGN for binding LARGE and enabling its  
363 function in the absence of phosphorylated core M3. Solution NMR studies reveal that LARGE  
364 has an increased binding affinity for core M3 when the core M3 mannose is phosphorylated, and  
365 the increased binding affinity of LARGE for the phosphorylated core M3 likely underlies the

366 ability of LARGE to synthesize full-length and high molecular weight matriglycan. The  
367 phosphorylated core M3, could therefore, serve to recruit LARGE, bound to DGN, to its acceptor  
368 oligosaccharide, where LARGE can generate full-length matriglycan. Taken together, these  
369 results indicate that LARGE requires DGN to synthesize the short, non-extended form of  
370 matriglycan but needs both the DGN and the phosphorylated core M3 to generate full-length  
371 matriglycan on  $\alpha$ -DG.

372 Our study demonstrates that POMK is required for the synthesis of full-length and high-  
373 molecular weight forms of matriglycan (**Figure 8- Figure Supplement 2A**). In the absence of  
374 POMK, LARGE generates a short, non-extended form of matriglycan (**Figure 8- Figure  
375 Supplement 2B**). Collectively, our work provides the first insights into the pathogenic  
376 mechanism behind POMK-deficient muscular dystrophy and better elucidates how full-length  
377 matriglycan is synthesized so it can act as a scaffold for ECM proteins, thereby enabling proper  
378 skeletal muscle function and preventing muscular dystrophy.

379 **Methods**

380

381 **Patient Information** Patient NH13-284 received a diagnosis of congenital muscular dystrophy  
382 (CMD) with brain malformations.

383 **Generation of POMK<sup>LoxP/LoxP</sup> Mice**

384 The *POMK* gene consists of five exons, exons 1, 2, and 3, which are non-coding and exons 4 and  
385 5, which are coding (*Zhu et al., 2016; Di Costanzo et al., 2014*). We used Clustered Regularly  
386 Interspersed Short Palindromic Repeats (CRISPR)-Cas9 to insert LoxP sites around *exon 5*.

387 *POMK\_5P1* TTCTTTCTGTGATGTGTGCTTATTCT

388 *POMK\_5P2* CAGACACTCACCCCTTACCTTAG

389 Wildtype: 197 bp

390 Targeted: 235 bp

391

392 *POMK\_3P1* AGCCACACCTTCCTACAGTC

393 *POMK\_3P2* AAGCTCTGCCAGAGAGAAG

394 Wildtype: 123 bp

395 Targeted: 162 bp

396

397 *POMK\_5'\_guide(601)* CGTGTCCCGCCAGGAATGAA

398 *POMK\_3'\_guide(3P1)* TCAGGAGGCGGCTCCCAGTG

399

400 *POMK\_5'\_donor(601; PAGE purified)*

401 TCCTCATCTTCTCCCTGTGCAGTCATCTGCACAGCTCCCTGCACACATGGCTTATAG

402 AGTGGTTCTCACCCGCCCTCATAACTCGTATAGCATACATTATACGAAGTTATG

403 GTACCTCCTGGCGGGACACGAATAAGCACACATCACAGAAAGTCTGTTGTCTT

404 GACTGCCAGCCCTCCGAGCTGCCACCC

405 *POMK\_3'\_donor(3P1; PAGE purified)*

406 AGTGTGAGATTCAAGTGTGGATATGCAGTGATCCTCTGGCCACACTTGTGAGCAGCC

407 ACACCTTCCTACAGTCCTCACTATAACTTCGTATAGCATACATTATACGAAGTTATG

408 GATCCGGGAGCCGCCTCCTGAGCCCTGCTGTGTAACCCACCTACCTCCCTCCTTCA

409 CACTAGAAGCTGAGAGCTTCTCTTC

410

411 **Animals**

412 B6SJLF1/J mice were purchased from Jackson Labs (100012; Bar Harbor, ME). Male mice older  
413 than 8 weeks were used to breed with 3-5-week-old super-ovulated females to produce zygotes for  
414 electroporation. Female ICR (Envigo, Indianapolis, IN; Hsc:ICR(CD-1)) mice were used as

415 recipients for embryo transfer. All animals were maintained in a climate-controlled environment  
416 at 25°C and a 12/12 light/dark cycle. Animal care and procedures were approved by and conformed  
417 to the standards of the Institutional Animal Care and Use Committee of the Office of Animal  
418 Resources at the University of Iowa.

419 **Preparation of Cas9 RNPs and the microinjection mix**

420 Chemically modified CRISPR-Cas9 crRNAs and CRISPR-Cas9 tracrRNAs were purchased from  
421 Integrated DNA Technologies (IDT) (Alt-R® CRISPR-Cas9 crRNA; Alt-R® CRISPR-Cas9  
422 tracrRNA (Cat# 1072532)). The crRNAs and tracrRNA were suspended in T10E0.1 and combined  
423 to 1 µg/µL (~29.5 µM) final concentration in a 1:2 (µg: µg) ratio. The RNAs were heated at 98°C  
424 for 2 minutes and allowed to cool slowly to 20°C in a thermal cycler. The annealed cr:tracrRNAs  
425 were aliquoted to single-use tubes and stored at -80°C.

426 Cas9 nuclease was also purchased from IDT (Alt-R® S.p. HiFi Cas9 Nuclease). Cr:tracr:Cas9  
427 ribonucleoprotein complexes were made by combining Cas9 protein and each cr:tracrRNA; final  
428 concentrations: 60 ng/µL (~0.4 µM) Cas9 protein and 60 ng/µL (~1.7 µM) cr:tracrRNA). The  
429 Cas9 protein and annealed RNAs were incubated at 37°C for 10 minutes. The two RNP mixes  
430 were combined and incubated at 37°C for an additional 5 minutes. The single stranded  
431 oligonucleotide donors (ssODN) were purchased from IDT as Ultramers. The ssODNs were added  
432 to the RNPs and the volume adjusted to the final concentrations in the injection mix were 10 ng/µL  
433 each ssODN; 20 ng/µL each guide RNA and 40 ng/µL Cas9 Protein.

434 **Collection of embryos and microinjection**

435 Pronuclear-stage embryos were collected using previously described methods (*Pinkert et al.,*  
436 *2002*). Embryos were collected in KSOM media (Millipore, Burlington, MA; MR101D) and  
437 washed 3 times to remove cumulous cells. Cas9 RNPs and ssODNs were injected into the pronuclei

438 of the collected zygotes and incubated in KSOM with amino acids at 37°C under 5% CO<sub>2</sub> until all  
439 zygotes were injected. Fifteen to 25 embryos were immediately implanted into the oviducts of  
440 pseudo-pregnant ICR females.

441 Insertion of loxP1 (5') and loxP2 (3') sites was confirmed by cloning and sequencing of genomic  
442 PCR products (Figure S2) from tail DNA of filial 0 (F0) POMK<sup>LoxP/+</sup> mice using primers flanking  
443 the 5' LoxP site, ACTCCAGTTGGTTTCAGGAAG and GAGGGAAGAGAAGTCAGGAAAG.  
444 For the 3' LoxP site, primers of sequence ACCGAGTGTGAGATTCAAGTG and  
445 GGTTGCTGGTAGGGTTAACAGAG were used. The 5' LoxP site contains a *KpnI* cleavage site,  
446 and the 3' LoxP site contains a *BamH*I site. The screen of the 5' LoxP site gives a product of 803  
447 base pairs for the LoxP allele when uncut. *KpnI* digestion of the 5' LoxP site gives 3 products of  
448 381, 355, and 67 base pairs. A screen of the 3' LoxP site gives a product of 396 base pairs for the  
449 uncut allele with LoxP site, while *BamH*I digestion of the 3' LoxP site gives products of 273 and  
450 123 base pairs.

451 Genotyping was carried out using primers flanking the exon 5 loxP1 site or the  
452 (TTCTTCTGTGATGTGTGCTTATTG) or loxP2 (CAGACACTCACCCTTACCTTAG) site.  
453 The wild-type allele is 197 bp while the floxed allele is 235 bp. POMK<sup>LoxP/+</sup> mice were backcrossed  
454 five generations onto a C57BL6/J background and backcrossed mice used whenever possible.  
455 Mice expressing Cre under the Mouse Creatine Kinase (MCK) promoter, B6.FVB(129S4)-  
456 Tg(Ckmm-cre)5Khn/J (stock no. 006475) (**Brüning et al., 1998**) and the Pax7-Cre promoter,  
457 Pax7<sup>tm1(cre)Mrc</sup>/J, (stock no. 010530) (**Keller et al., 2004**) were purchased from the Jackson  
458 Laboratory. Male mice expressing the MCK-Cre transgene were bred to female mice homozygous  
459 for the floxed *POMK* allele (POMK<sup>LoxP/LoxP</sup>). Male F1 progeny with the genotype MCK-Cre;  
460 POMK<sup>LoxP/+</sup> were bred to female POMK<sup>LoxP/LoxP</sup> mice. A Cre PCR genotyping protocol was used

461 to genotype the Cre allele using standard Cre primers. The primers used were Sense:  
462 TGATGAGGTTCGCAAGAAC and Antisense: CCATGAGTGAACGAACCTGG.  
463 Sanger sequencing of tail DNA was performed by the University of Iowa Genome Editing Core  
464 Facility to confirm incorporation of 5' and 3' LoxP sites. PCR probes were developed at  
465 Transnetyx to genotype mice expressing both Pax7-Cre and MCK-Cre. Genotyping of MCK-Cre;  
466 Pax7-Cre; POMK<sup>LoxP/LoxP</sup> mice was performed by Transnetyx using real-time PCR.  
467 All mice were socially housed in a barrier-free, specific pathogen-free conditions as approved by  
468 the University of Iowa Animal Care and Use Committee (IACUC). Animal care, ethical usage,  
469 and procedures were approved and performed in accordance with the standards set forth by the  
470 National Institutes of Health and IACUC. For studies with MCK-Cre; POMK<sup>LoxP/LoxP</sup> mice, N=3  
471 mice of each genotype (POMK<sup>LoxP/LoxP</sup> and MCK-Cre; POMK<sup>LoxP/LoxP</sup>) were used. For studies with  
472 MCK-Cre; Pax7-Cre; POMK<sup>LoxP/LoxP</sup> mice, animals of varying ages were used as indicated, and  
473 N=3 each of POMK<sup>LoxP/LoxP</sup> and MCK-Cre; Pax7-Cre; POMK<sup>LoxP/LoxP</sup> were used. Littermate  
474 controls were employed whenever possible.

475 **Forelimb Grip Strength Test**

476 Forelimb grip strength was measured at 4 weeks of age. A mouse grip strength meter (Columbus  
477 Instruments, Columbus, OH) was mounted horizontally, with a nonflexible grid connected to the  
478 force transducer. The mouse was allowed to grasp the grid with its two front paws and then pulled  
479 away from the grid by its tail until the grip was broken. This was done three times over five trials,  
480 with a one-minute break between each trial. The gram force was recorded per pull, and any pull  
481 where only one front limb or any hind limbs were used were discarded. If the mouse turned, the  
482 pull was also discarded. After 15 pulls (5 sets of 3 pulls), the mean of the three highest pulls of the  
483 15 was calculated and reported. Statistics were calculated using GraphPad Prism 8 software.

484 Student's T-Test was used (two-sided). Differences were considered significant at a p-value less  
485 than 0.05. Graph images were also created using GraphPad Prism and the data in the present study  
486 are shown as the means +/- SD unless otherwise indicated.

487 **Creatine Kinase Assay**

488 Creatine Kinase levels were measured in 8-week old mice 2 hours after mild downhill run (3 meters  
489 per minute for 5 minutes followed by 15 meters per minute for 10 minutes) at a 15- degree downhill  
490 incline. Blood was collected by tail vein bleeds from non-anesthetized, restrained mice using a  
491 Microvette CB300 (Sarstedt AG & Co, Newton, NC). Samples were centrifuged at 12,000 rpm for  
492 10 minutes and prepared using an enzyme-coupled CK kit (Stanbio Laboratory, Boerne, TX) using  
493 the manufacturer's instructions. Absorbance was measured using a plate reader at 340 nm every  
494 30 seconds for 2 minutes at 37°C. Statistics were calculated using GraphPad Prism software and  
495 Student's T-Test was used (two-sided). Differences were considered significant at a p-value less  
496 than 0.05. Graph images were also created using GraphPad Prism 8 and the data in the present  
497 study are shown as the means +/- SD unless otherwise indicated.

498 **Body Weight Measurements**

499 Mice were weighed after measuring grip strength using a Scout SPX222 scale (OHAUS  
500 Corporation, Parsippany, NJ), and the tester was blinded to genotype. Statistics were calculated  
501 using GraphPad Prism 8 software and Student's T-Test was used (two-sided). Differences were  
502 considered significant at a p-value less than 0.05. Graph images were also created using GraphPad  
503 Prism and the data in the present study are shown as the means +/- SD unless otherwise indicated.

504 **Measurement of *in vitro* muscle function**

505 To compare the contractile properties of muscles, extensor digitorum longus (EDL) muscles were  
506 surgically removed as described previously (**Rader et al., 2016**). The muscle was immediately  
507 placed in a bath containing a buffered physiological salt solution (composition in mM: NaCl, 137;  
508 KCl, 5; CaCl<sub>2</sub>, 2; MgSO<sub>4</sub>, 1; NaH<sub>2</sub>PO<sub>4</sub>, 1; NaHCO<sub>3</sub>, 24; glucose, 11). The bath was maintained  
509 at 25°C, and the solution was bubbled with 95% O<sub>2</sub> and 5% CO<sub>2</sub> to stabilize pH at 7.4. The  
510 proximal tendon was clamped to a post and the distal tendon tied to a dual mode servomotor  
511 (Model 305C; Aurora Scientific, Aurora, ON, Canada). Optimal current and whole muscle length  
512 (L<sub>0</sub>) were determined by monitoring isometric twitch force. Optimal frequency and maximal  
513 isometric tetanic force (F<sub>0</sub>) were also determined. The muscle was then subjected to an eccentric  
514 contraction (ECC) protocol consisting of 8 eccentric contractions (ECCs) at 3-minute intervals. A  
515 fiber length (L<sub>f</sub>)-to-L<sub>0</sub> ratio of 0.45 was used to calculate L<sub>f</sub>. Each ECC consisted of an initial 100  
516 millisecond isometric contraction at optimal frequency immediately followed by a stretch of L<sub>0</sub> to  
517 30% of L<sub>f</sub> beyond L<sub>0</sub> at a velocity of 1 L<sub>f</sub>/s at optimal frequency. The muscle was then passively  
518 returned to L<sub>0</sub> at the same velocity. At 3, 15, 30, 45, and 60 minutes after the ECC protocol,  
519 isometric tetanic force was measured. After the analysis of the contractile properties, the muscle  
520 was weighed. The cross-sectional area (CSA) of muscle was determined by dividing the muscle  
521 mass by the product of L<sub>f</sub> and the density of mammalian skeletal muscle (1.06 g/cm<sup>3</sup>). The specific  
522 force was determined by dividing F<sub>0</sub> by the CSA (kN/mm<sup>2</sup>). 18-20 week-old male mice were used,  
523 and right and left EDL muscles from each mouse were employed whenever possible, with n=5 to  
524 8 muscles used for each analysis. Each data point represents an individual EDL. Statistics were  
525 calculated using GraphPad Prism 8 software and Student's unpaired T-Test was used (two-sided).  
526 Differences were considered significant at a p-value less than 0.05.

527 **H&E and Immunofluorescence Analysis of Skeletal Muscle**

528 Histology and immunofluorescence of mouse skeletal muscle were performed as described  
529 previously (*Goddeeris et al., 2013*). Mice were euthanized by cervical dislocation and directly after  
530 sacrifice, quadriceps muscles were isolated, embedded in OCT compound and then snap frozen in  
531 liquid nitrogen cooled 2-methylbutane. 10  $\mu$ M sections were cut with a cryostat (Leica CM3050S  
532 Research Cryostat; Amsterdam, the Netherlands) and H&E stained using conventional methods.  
533 Whole digital images of H&E-stained sections were taken by a VS120-S5-FL Olympus slide  
534 scanner microscope (Olympus Corporation, Tokyo, Japan). For immunofluorescence analyses, a  
535 mouse monoclonal antibody to glycoepitopes on the sugar chain of  $\alpha$ -DG (IIH6, 1:100 dilution,  
536 Developmental Studies Hybridoma Bank, University of Iowa; RRID: AB\_2617216) was added to  
537 sections overnight at 4°C followed by Alexa Fluor®-conjugated goat IgG against mouse IgM  
538 (Invitrogen, Carlsbad, CA, 1:500 dilution), for 40 minutes. The sections were also stained with  
539 rabbit polyclonal antibody to  $\beta$ -DG (AP83; 1:50 dilution) followed by Alexa Fluor®-conjugated  
540 488 Goat anti-rabbit IgG (1:500). Whole sections were imaged with a VS120-S5-FL Olympus  
541 slide scanner microscope. Antibody IIH6 is a monoclonal to the glycoepitope of  $\alpha$ -DG (*Ervasti et*  
542 *al., 1991*), and AP83 is a polyclonal antibody to the c-terminus of  $\beta$ -DG (*Ervasti et al., 1991*), both  
543 of which have been described previously.

544 For histologic analysis of human skeletal muscle, H&E staining on 10  $\mu$ m frozen section was  
545 performed using the Leica ST5020 Multistainer workstation (Leica Biosystems, Buffalo Grove,  
546 IL) according manufacturer's instructions. For immunofluorescence analysis, unfixed frozen serial  
547 sections (7  $\mu$ m) were incubated with primary antibodies for 1 hour, and then with the appropriate  
548 biotinylated secondary antibodies for 30 minutes followed by streptavidin conjugated to Alexa  
549 Fluor 594 (ThermoFisher Scientific, UK) for 15 minutes. Primary antibodies used were mouse

550 monoclonal:  $\alpha$ -DG IIH6 (clone IIH6C4) (**Ervasti et al., 1991**),  $\beta$ -DG (Leica, Milton Keynes, UK;  
551 clone 43DAG1/8D5). All washes were made in PBS and incubations were performed at room  
552 temperature. Sections were evaluated with a Leica DMR microscope interfaced to MetaMorph  
553 (Molecular Devices, Sunnyvale, CA).

554 **Tissue Biochemical Analysis**

555 30 slices of 30  $\mu$ M thickness were taken with a with a cryostat (Leica CM3050S Research  
556 Cryostat) from skeletal muscle or heart that had been frozen in liquid nitrogen-cooled 2-  
557 methylbutane. For biochemical analysis of murine skeletal muscle, quadriceps muscle were used.  
558 Samples were solubilized in 500  $\mu$ L of 1% Triton X-100 in 50 mM Tris pH 7.6 and 150 mM NaCl  
559 with protease inhibitors (per 10 mL buffer: 67  $\mu$ L each of 0.2 M Phenylmethylsulfonylfluoride  
560 (PMSF), 0.1 M Benzamidine and 5  $\mu$ L of each of Leupeptin (Sigma/Millipore) 5 mg/mL, Pepstatin  
561 A (Millipore) 1 mg/mL in methanol, Aprotinin (Sigma-Aldrich) 5 mg/mL, Calpeptin (Fisher/EMD  
562 Millipore) 1.92 mg/mL in Dimethyl Sulfoxide (DMSO), Calpain Inhibitor 1 (Sigma-Aldrich) 1.92  
563 mg/mL in DMSO). Samples were vortexed for 4 minutes and solubilized for 2.5 hours at 4°C with  
564 rotation. Samples were then spun down at 12,000 rpm for 30 minutes at 4°C on a Beckman  
565 Tabletop Centrifuge. The supernatant was incubated with 100  $\mu$ L WGA-Agarose slurry (Vector  
566 Biolabs, Malvern, PA, AL-1023) overnight at 4°C with rotation. The next day samples were  
567 washed three times in 50 mM Tris pH 7.6 and 150 mM NaCl with 0.1% TX-100 and protease  
568 inhibitors. 100  $\mu$ L of 5X Laemmli Sample Buffer (LSB) was added, samples boiled for 10 minutes,  
569 and 125  $\mu$ L of this was loaded in each lane of gels for western blotting.

570 **Fibroblast Growth and Flow Cytometry**

571 Fibroblasts used for biochemical analyses were grown in 20% Fetal Bovine Serum (FBS, Life  
572 Technologies, Carlsbad, CA) and 1% penicillin/streptomycin (Invitrogen). Cells were split at 1:2  
573 every 2 days using Trypsin-EDTA (ThermoFisher Scientific, Waltham, MA).  
574 For flow cytometry analyses, fibroblasts cultured from skin biopsies were grown in Dulbecco's  
575 modified Eagles medium (Invitrogen) with 20% fetal bovine serum (FBS, Life Technologies), 1%  
576 glutamax (Thermo Fisher Scientific) and 1% penicillin/streptomycin (Sigma-Aldrich). Upon  
577 approximately 90% confluence, cells were washed with PBS without Ca and Mg, detached with  
578 non-enzymatic dissociation solution (Sigma-Aldrich cat. C5914) and fixed in 2%  
579 paraformaldehyde for 10 minutes. Cells were subsequently incubated on ice with the following  
580 antibodies diluted in PBS/0.1% FBS: anti- $\alpha$ -DG IIH6 (Millipore) for 30 minutes, anti-mouse  
581 biotinylated IgM (Vector Labs, Burlingame, CA) for 20 minutes, Streptavidin-Phycoerythrin (BD  
582 Pharmingen) for 15 minutes. Negative controls for each fibroblast population were incubated with  
583 0.1% FBS/PBS without the primary antibodies. Cells were washed twice and centrifuged at 1850g  
584 for 4 minutes, after each incubation step. After the last wash, cell pellets were re-suspended in 500  
585  $\mu$ L of PBS. A total of 10,000 event were acquired using the Cyan ADP analyser (Beckman Coulter,  
586 Brea, CA) and analysed using FlowJo software version 7.6.5 (Tree Star, USA).

587 **Generation and Characterization of HAP1 Mutant Cell Lines**

588 HAP1 cells (RRID: CVCL\_Y019) are a haploid human cell line with an adherent, fibroblast-like  
589 morphology, originally derived from parent cell line KBM-7 (RRID: CVCL\_A426). Wild-type  
590 C631 (a diploid cell line containing duplicated chromosomes of HAP1) were purchased from  
591 Horizon Discovery and gene-specific knockout HAP1 cells were generated by Horizon Discovery.

592 *POMK* knockout (KO) HAP1: HAP1 cells bearing a 10 bp deletion of exon 4 of the *POMK*,  
593 generated using the CRISPR/Cas9 system, were purchased from Horizon Discovery  
594 (HZGHC001338c004, clone 1338-4) and were previously described (Zhu *et al.*, 2016). *POMK*  
595 knockout (KO) HAP1 cells lack the single copy of the wild-type *POMK* allele and are therefore  
596 null at the *POMK* locus. The sequence of the guide RNA used is  
597 TGAGACAGCTGAAGCGTGTT. Absence of the wild-type *POMK* allele was confirmed by  
598 Horizon Discovery via PCR amplification and Sanger sequencing. PCR primers used for DNA  
599 sequencing are *POMK* Forward 5'-ACTTCTTCATCGCTCCTCGACAA-3', and *POMK*  
600 Backward 5'- GGATGCCACACTGCTCCCTAA-3'. The identity of the cells has been  
601 authenticated by the company using the STR profiling method. Mycoplasma testing of the cells  
602 were performed on a routine basis to ensure the cells are not contaminated.

603 *POMK/DG* KO HAP1: HAP1 cells lacking both *POMK* and *DAG1* expression (*POMK/DG* KO  
604 HAP1 cells) were generated using CRISPR/Cas9 by Horizon Discovery. A 16 bp deletion in the  
605 *DAG1* gene (exon 2) was introduced into the *POMK* KO HAP1 line (HZGHC001338c004). The  
606 sequence of the Guide RNA is CCGACGACAGCCGTGCCATC; NM\_004393. PCR primers for  
607 DNA sequencing were forward TAGCAAGACTATCGACTTGAGCAAA and reverse  
608 GCAATCAAATCTGTTGGAATGGTCA.

609 *POMK/LARGE* KO HAP1: HAP1 cells lacking both *POMK* and *LARGE* expression  
610 (*POMK/LARGE* KO HAP1 cells) (HZGHC007364c011) were generated using CRISPR/Cas9 by  
611 Horizon Discovery. A 43 bp deletion of exon 3 of *LARGE* was introduced into the *POMK* KO  
612 HAP1 line (HZGHC001338c004). The guide RNA sequence was  
613 CTCGGCGATGGATGGGGCT and the primer sequence was PCR forward

614 GAGGCATGGTTCATCCAGATTAAAG and PCR reverse  
615 CTTTACCTCGCATTCTCCACGA.

616 *POMK/ISPD* KO HAP1: HAP1 cells containing a 1 bp insertion of exon 4 of the *POMK* gene,  
617 generated using the CRISPR/Cas9 system, were purchased from Horizon Discovery  
618 (HZGHC001338c001, clone 1338–1). The mutation in *POMK* is predicted to lead to a frameshift.  
619 These cells also lacked expression of *ISPD*. The Guide RNA sequence was  
620 TGAGACAGCTGAAGCGTGTT. The sequences of PCR primers were PCR forward  
621 ACTTCTTCATCGCTCCTCGACAA and PCR reverse GGATGCCACACTGCTTCCCTAA.

622 *LARGE* KO HAP1: HAP1 cells (clone 122-6, HZGHC000122c006) were purchased from Horizon  
623 Discovery. Cells were generated using a CRISPR/Cas9-mediated 1 bp deletion of exon 3. The  
624 guide RNA sequence was GCTCTCGCGCTCCGCTGGC and the primer sequence for 122-7  
625 was PCR forward ATGGAGTAGGTCTTGGAGTGGTT and PCR reverse  
626 GAGGCATGGTTCATCCAGAGTTAAAG.

627 *FKTN* KO HAP1: HAP1 cells (clone 721-10, catalog number 32597-10) were purchased from  
628 Horizon Discovery. CRISPR/Cas9 was used to introduce 16 bp deletion of exon 3. The sequence  
629 of the guide RNA was CAGAACTTGTCAAGCGTTAAA and the sequences of PCR forward  
630 CAGATCAAAGAATGCCTGTGGAAAT and PCR reverse  
631 TGCAAAGAGAAGTGTGATCAGAAAA.

632 **Adenovirus Production**

633 DGE (Delta H30- A316) was generated and described previously (*Hara et al., 2011; Kanagawa et al., 2004; Kunz et al., 2001*). DG T317A, DG T319A, and DG T317A/T319A were first  
634 subcloned into an Fc-tagged DG construct (DGFc3) (*Hara et al., 2011; Kanagawa et al., 2004; Kunz et al., 2001*). The *KpnI-XhoI* fragments from the DGFc3 mutants corresponding to the mutant

637 constructs (DG T317A, DG T319A, or DG T317A/T319A) were then subcloned into pAd5RSVK-  
638 NpA (obtained from the University of Iowa Viral Vector Core) as was the *XhoI-XbaI* fragment  
639 from an adenovirus encoding dystroglycan-WT. *E1*-deficient recombinant adenoviruses (Ad5  
640 RSV DG-WT, DG T317/T319, DG T317A, DG T319A, DGE, Ad-*POMK* WT) were generated by  
641 the University of Iowa Viral Vector Core (VVC) using the RAPAd system (*Anderson et al., 2000*).  
642 Assays for replication competence of adenoviruses were performed to check for contamination.  
643 Ad-*POMK*-WT and Ad-*POMK*-D204A were generated by ViraQuest Inc. (North Liberty, IA)  
644 using the RAPAd system and was described previously (*Zhu et al., 2016*). Ad-*POMK*-D204N was  
645 also generated by ViraQuest Inc. Absence of the viral *E1* DNA sequence was confirmed by  
646 ViraQuest Inc. after PCR amplification of the viral DNA and staining on DNA agarose gel  
647 electrophoresis. Replication competence of adenoviruses was negative as assessed by plaque  
648 forming assays in cells performed from  $10^9$  viral particles up to 14 days. Adenoviral *Fukutin*  
649 (*FKTN*) and *Isoprenoid Synthase Domain-Containing* (*ISPD*) have been described previously  
650 (*Hara et al., 2011*). Adenoviral *LARGE* has been described previously (*Barresi et al., 2004*).  
651 DGFc340TEV was cloned into the pUC57-mini vector by GenScript (*Hara et al., 2011*;  
652 *Kanagawa et al., 2004; Kunz et al., 2001*). The insert includes TEV protein cleavage site between  
653 amino acids (AAs) 1-340 of rabbit DG and human IgG1 Fc. The insert was subcloned in pcDNA3  
654 expression vector with *EcoRI*. Subsequently, *FseI*-x-340 AAs DG-TEV-6xHis-*NotI* fragment was  
655 obtained using pcDNA3DGFc340TEV as a PCR template. *FseI*-x-340 AAs DG-TEV-6xHis-*NotI*  
656 was ligated into pcDNA3DGFc340TEV digested with *FseI* and *NotI* to construct DG340TEVHis,  
657 which includes 1-340 AAs of rabbit DG, TEV site, and 6x Histidine. The construct was also  
658 inserted in pacAd shuttle plasmid from the VVC to generate the adenoviral vector. Next, *FseI*-x-  
659 390 AAs-TEV-6xHis-*NotI* was obtained using pcDNA3rbtDG as a PCR template and ligated into

660 the pcDNA3DG340TEVHis digested with *FseI* and *NotI* to construct DG390TEVHis, which  
661 includes 1-390 AAs of rabbit DG, TEV site, and 6x Histidine. The construct was also inserted in  
662 pacAd shuttle plasmid from the VVC to generate the Ad virus vector. E1-deficient recombinant  
663 adenoviruses were generated by the University of Iowa Viral Vector Core using the RAPAd  
664 system (**Kunz et al., 2001**).

665 **HAP1 Cell Culture and Adenovirus Infection**

666 HAP1 cells were maintained at 37°C and 5% CO<sub>2</sub> in Iscove's Modified Dulbecco's Medium  
667 (IMDM, Gibco) supplemented with 10% Fetal Bovine Serum (FBS) and 1%  
668 penicillin/streptomycin (Invitrogen). Cells were split every 3 days at 1:10 using Trypsin-EDTA  
669 (ThermoFisher Scientific). On day 1, media was changed to 2% IMDM, and an average of 5.9 ×  
670 10<sup>6</sup> *POMK* KO HAP1 cells were infected at the indicated multiplicity of infection (MOI) of the  
671 indicated adenovirus. On day 2, infection medium was replaced with 10% IMDM, and on day  
672 three the cells were processed for biochemical analyses.

673 **Glycoprotein Isolation and Biochemical Analyses from Cultured Cells**

674 For western blots and laminin overlay, HAP1 cells and fibroblasts were washed twice in ice-cold  
675 Dulbecco's Phosphate-Buffered Saline (DPBS, Gibco). The second PBS wash contained the  
676 protease inhibitors (0.23 mM PMSF and 0.64 mM Benzamidine). Plates were scraped, spun down  
677 for 5 minutes at 14, 000 rpm at 4°C, and pellets were solubilized in 1% Triton X-100 in Tris-  
678 buffered saline (TBS, 50 mM Tris-HCl pH 7.6, 150 mM NaCl) with protease inhibitors (0.23 mM  
679 PMSF and 0.64 mM Benzamidine) for 1 hour at 4°C. Samples were then spun down at 14,000 rpm  
680 for 5 minutes, and supernatants incubated in 200 µL wheat-germ agglutinin (WGA)-agarose  
681 (Vector Laboratories, AL-1023) as previously described (**Michele et al., 2002; Goddeeris et al.,**  
682 **2013**). The following day, WGA beads were washed three times with 0.1% Triton X-100-TBS

683 plus protease inhibitors and heated to 99°C for 10 minutes with 250 µL of 5X Laemmli sample  
684 buffer. Samples were run on SDS-PAGE and transferred to PVDF-FL membranes (Millipore) as  
685 previously published (*Michele et al., 2002; Goddeeris et al., 2013*).

686 **Immunoblotting and Ligand Overlay**

687 The mouse monoclonal antibody against  $\alpha$ -DG (IIH6, Developmental Studies Hybridoma Bank,  
688 University of Iowa; RRID: AB\_2617216) was characterized previously and used at 1:100 (*Ervasti  
et al., 1991*). The polyclonal antibody, AF6868 (R&D Systems, Minneapolis, MN; RRID:  
690 AB\_10891298), was used at a concentration of 1:200 for immunoblotting the core  $\alpha$ -DG and  $\beta$ -  
691 DG proteins, and the secondary was a Donkey anti-Sheep (LI-COR Bioscience, Lincoln, NE) used  
692 at 1:2000 concentration. Anti-POMK (Novus Biologicals, Littleton, CO, 6f10) was used at 1:500,  
693 and the secondary was 1:2000 Goat anti-Mouse IgG1 (LI-COR Bioscience). The antibody against  
694 the Na/K ATPase (BD Biosciences, San Jose, CA, 610993) was used at 1:1000 in 5%-milk Blotto,  
695 and the secondary was 1:10,000 Goat anti-Mouse IgG1 (LI-COR Bioscience). Anti-myc (Millipore  
696 Sigma, Clone 4A6) was used at 1:2,000 in 2% milk and the secondary was 1:2,000 Goat anti-  
697 Mouse IgG1 (LI-COR Bioscience). Blots were developed with infrared (IR) dye-conjugated  
698 secondary antibodies (LI-COR Bioscience) and scanned using the Odyssey infrared imaging  
699 system (LI-COR Bioscience). Blot images were captured using the included Odyssey image-  
700 analysis software.

701 Laminin overlay assays were performed as previously described (*Michele et al., 2002; Goddeeris  
et al., 2013*). PVDF-FL membranes were blocked in laminin binding buffer (LBB: 10 mM  
703 triethanolamine, 140 mM NaCl, 1 mM MgCl<sub>2</sub>, 1 mM CaCl<sub>2</sub>, pH 7.6) containing 5% milk followed  
704 by incubation with mouse Engelbreth-Holm-Swarm (EHS) laminin (ThermoFisher, 23017015)  
705 overnight at a concentration of 7.5 nM at 4°C in LBB containing 3% bovine serum albumin (BSA)

706 and 2 mM CaCl<sub>2</sub>. Membranes were washed and incubated with anti-laminin antibody (L9393;  
707 Sigma-Aldrich 1:1000 dilution) followed by IRDye 800 CW dye-conjugated donkey anti-rabbit  
708 IgG (LI-COR, 926-32213) at 1:2500 dilution.

709 **EDTA Treatment of Ligand Overlays**

710 EDTA treatment of laminin overlay assays were performed as described above for laminin  
711 overlays; however, calcium was excluded from all buffers made with LBB (i.e. 5% milk-LBB, 3%  
712 BSA-LBB) and 10 mM EDTA was added to all LBB-based buffers, including LBB wash buffer,  
713 5% milk-LBB, and 3% BSA-LBB buffers.

714 **POMK Assay**

715 HAP1 cells were washed twice in ice-cold PBS, scraped, and spun down at 14,000 rpm for 5  
716 minutes at 4°C. After removing supernatant, the cell pellet was resuspended in 0.1 M MES buffer  
717 pH 6.5 with 1% Triton X-100 with Protease Inhibitors (0.23 mM PMSF and 0.64 mM  
718 Benzamidine) for 1 hour at 4°C rotating. Samples were spun down again, and the supernatant was  
719 incubated with 200 µL of WGA-agarose beads (Vector Biolabs, AL-1023) overnight at 4°C with  
720 rotation. Samples were washed the next day three times in 0.1 M MES pH 6.5 with 0.1% Triton  
721 X-100 and protease inhibitors, and 100 µL of the beads were resuspended in 100 µL of the wash  
722 buffer.

723 For fibroblast POMK activity measurements, cells were processed as above and solubilized in 1%  
724 TX-100 in 50 mM Tris and 150 mM NaCl pH 7.6 with protease inhibitors as described above and  
725 incubated with WGA-agarose beads. The next day, WGA beads were washed three times and  
726 resuspended in 0.1% TX-100 in 0.1 M MES pH 6.5 buffer with protease inhibitors.

727 For measurement of mouse and human skeletal muscle POMK activity, 30 slices of 30 µM  
728 thickness were taken using a Leica 3050s cryostat from quadriceps muscle frozen in liquid

729 nitrogen-cooled 2-methylbutane. Samples were solubilized in 250  $\mu$ L of 1% Triton X-100 in 0.1  
730 M MES pH 6.5 with protease inhibitors (per 10 mL buffer: 67  $\mu$ L each of 0.2 M PMSF, 0.1 M  
731 Benzamidine and 5  $\mu$ L/10 mL of buffer of Leupeptin (Sigma/Millipore) 5 mg/mL, Pepstatin A  
732 (Millipore) 1 mg/mL in methanol, Aprotinin (Sigma-Aldrich) 5 mg/mL, Calpeptin (Fisher/EMD  
733 Millipore) 1.92 mg/mL in Dimethyl Sulfoxide (DMSO), Calpain Inhibitor 1 (Sigma-Aldrich) 1.92  
734 mg/mL in DMSO). Samples were solubilized for 2.5 hours at 4°C on a rotator. Samples were then  
735 spun down at 14, 000 rpm for 30 minutes at 4°C on a Beckman Tabletop Centrifuge. The  
736 supernatant (total lysate) was separated from the pellet, and 10  $\mu$ L of this was used for POMK  
737 assays.

738 For POMK reaction in HAP1 cells and fibroblasts, 20  $\mu$ L slurry (consisting of 10  $\mu$ L beads and 10  
739  $\mu$ L MES buffer) was incubated with reaction buffer for a final reaction volume of 40  $\mu$ L. For  
740 POMK assay from skeletal muscle, 10  $\mu$ L of total lysate was incubated with 20  $\mu$ L of reaction  
741 buffer for a reaction volume of 30  $\mu$ L. The final reaction concentration was 10 mM ATP, 10 mM  
742 MnCl<sub>2</sub>, 10 mM MgCl<sub>2</sub>, 10  $\mu$ M GGM-MU, 0.1% TX-100 in 0.1 M MES Buffer pH 6.5. Reactions  
743 were run at 37°C for 24 hours for HAP cells, 48 hours for fibroblasts, or 16 hours for skeletal  
744 muscle. Experiments were done in triplicate, with each replicate representing a separate plate of  
745 cells or animal. After POMK reaction, 6  $\mu$ L 0.5 M EDTA was added to 30  $\mu$ L of reaction  
746 supernatant, and the mixture boiled for 5 minutes. 25  $\mu$ L of this mixture and added to 30  $\mu$ L ddH<sub>2</sub>O  
747 in HPLC vial and run on an LC18 column of a reverse-phase HPLC (Shimadzu Scientific,  
748 Columbia, Maryland) with a 16% B med sensitivity gradient. The reaction was analyzed using a  
749 4.6 x 250 mm Supelcosil LC-18 column (Supelco). Solvent A was 50 mM ammonium formate  
750 (pH 4.0), and solvent B was 80% acetonitrile in solvent A. Elution of the MU derivative was  
751 monitored by fluorescence detection (325 nm for excitation, and 380 nm for emission) and peak

752 area used as a measure of activity. The enzymatic activity was calculated as the peak area of the  
753 product.

754 **B4GAT1 Assay**

755 For the assessment of endogenous B4GAT1 activity in skeletal muscle, Triton X-100-solubilized  
756 lysates (10  $\mu$ l for human skeletal muscle or 40  $\mu$ L for mouse skeletal muscle) were incubated in a  
757 volume of 50  $\mu$ L (human skeletal muscle) for 12 hours at 37°C, with 0.4 mM Xylose- $\beta$ -MU (Xyl-  
758  $\beta$ -MU) and 10 mM Uridine diphosphate glucuronic acid (UDP-GlcA) in 0.1 M MES buffer, pH  
759 6.0, at 5 mM MnCl<sub>2</sub>, 5 mM MgCl<sub>2</sub>, and 0.05% Triton X-100 (*Willer et al., 2014*). The reaction  
760 was terminated by adding 25  $\mu$ L of 0.1 M EDTA and boiling for 5 minutes, and the supernatant  
761 was analyzed using an LC-18 column. Both the substrate Xyl- $\beta$ -MU and the product GlcA-Xyl- $\beta$ -  
762 MU were separated on a 16% acetonitrile isocratic gradient. Elution of the MU derivative product  
763 was monitored by fluorescence detection (325 nm for excitation, and 380 nm for emission). The  
764 percent conversion of substrate to product was used as the activity of the B4GAT1 in the 10  $\mu$ L  
765 sample. The B4GAT1 activity then was normalized against the amount of protein measured in the  
766 10  $\mu$ L of sample using the DC Protein Assay (Bio-Rad, Hercules, CA) with BSA as the standard.  
767 For assessment of B4GAT1 activity in HAP cells, the HAP WGA beads were incubated in a  
768 volume of 80  $\mu$ L for 26 h at 37°C, with 0.4 mM Xyl- $\beta$ -MU and 10 mM UDP-GlcA in 0.1 M MES  
769 buffer, pH 6.0, at 5 mM MnCl<sub>2</sub>, 5 mM MgCl<sub>2</sub>, and 0.05% Triton X-100. The reaction was  
770 terminated by adding 25  $\mu$ L of 0.1 M EDTA and boiling for 5 minutes, and the supernatant was  
771 analyzed using an LC-18 column. Elution of the MU derivative was monitored by fluorescence  
772 detection (325 nm for excitation, and 380 nm for emission) and peak area used as a measure of  
773 activity. The percent product was determined by taking the product peak area and dividing by the

774 total peak areas of substrate plus product peak. Then this number was taken and multiplied by 100  
775 for percent conversion to product.

776 **LARGE Assay**

777 For the assessment of endogenous LARGE GlcA-T activity in skeletal muscle, Triton X-100-  
778 solubilized lysates were incubated in a volume of 25  $\mu$ L for 3 h at 37°C, with 0.4 mM Xyl- $\alpha$ 1,3-  
779 GlcA- $\beta$ -MU and 10 mM UDP-GlcA in 0.1 M MES buffer, pH 6.0, at 5 mM MnCl<sub>2</sub>, 5 mM MgCl<sub>2</sub>,  
780 and 0.5% Triton X-100. The reaction was terminated by adding 25  $\mu$ L of 0.1 M EDTA and boiling  
781 for 5 minutes, and the supernatant was analyzed using an LC-18 column. Elution of the MU  
782 derivative was monitored by fluorescence detection (325 nm for excitation, and 380 nm for  
783 emission) and peak area used as a measure of activity. The GlcA-T activity was assessed by  
784 subtracting the background observed in the negative control sample without donor sugar and  
785 normalized against the amount of protein measured using the DC Protein Assay (Bio-Rad).

786 For assessment of LARGE enzymatic activity in HAP cells, the Triton X-100 solubilized HAP  
787 cells were loaded onto WGA beads and processed as described for POMK assay above. The next  
788 day after wash, beads were incubated in a volume of 90  $\mu$ L with 0.4 mM Xyl- $\alpha$ 1,3-GlcA- $\beta$ -MU  
789 and 10 mM UDP-GlcA in 0.1 M MOPS buffer, pH 6.0, at 5 mM MnCl<sub>2</sub>, 5 mM MgCl<sub>2</sub>, and 0.05%  
790 Triton X-100. The samples were run for 46 h at 37°C. The reaction was terminated by adding 25  
791  $\mu$ L of 0.25 M EDTA and boiling for 5 minutes, and the supernatant was analyzed using an LC-18  
792 column.

793 For the assessment of endogenous LARGE activity in fibroblasts, supernatants from Triton X-100  
794 solubilized fibroblasts were (20  $\mu$ L) directly used. Supernatants were incubated in a volume of 100  
795  $\mu$ L for 24 h at 37°C, with 0.4 mM Xyl- $\alpha$ 1,3-GlcA- $\beta$ -MU and 10 mM UDP-GlcA in 0.1 M MES  
796 buffer, pH 6.0, at 5 mM MnCl<sub>2</sub>, 5 mM MgCl<sub>2</sub>, and 0.5% Triton X-100. The reaction was

797 terminated by adding 25  $\mu$ L of 0.1 M EDTA and boiling for 5 minutes, and the supernatant was  
798 analyzed using an LC-18 column.

799 Elution of the MU derivative was monitored by fluorescence detection (325 nm for excitation, and  
800 380 nm for emission) and peak area used as a measure of activity. The percent product was  
801 determined by taking the product peak area and dividing by the total peak areas of substrate plus  
802 product peak. Then this number was taken and multiplied by 100 for percent conversion to product.

803 **B3GALNT2 Assay**

804 To assess B3GALNT2 activity in HAP1 cells, 20  $\mu$ L of the WGA beads from HAP1 cells were  
805 incubated with a 20  $\mu$ L volume of the reaction mix. The final volume of reaction buffer was 40  
806  $\mu$ L (30  $\mu$ L reaction mixture and 10  $\mu$ L WGA-beads). The final concentrations were 10 mM MgCl<sub>2</sub>,  
807 10 mM MnCl<sub>2</sub>, 0.1 M MES pH 6.5, 10  $\mu$ M GGM-MU, and 10 mM UDP-GlcNac. Reactions were  
808 run at 37°C for 72 hours. Experiments were done in triplicate, with each replicate representing a  
809 separate plate of cells. After B3GALNT2 reaction, 6  $\mu$ L 0.5 M EDTA was added to 30  $\mu$ L of  
810 reaction supernatant, and the mixture boiled for 5 minutes. 25  $\mu$ L of this mixture and added to 30  
811  $\mu$ L ddH<sub>2</sub>O in HPLC vial and run on an LC18 column of a reverse-phase HPLC (Shimadzu  
812 Scientific) with a 16% B med sensitivity gradient. The reaction was analyzed using a 4.6 x 250  
813 mm Supelcosil LC-18 column (Supelco, Bellefonte, PA). Solvent A was 50 mM ammonium  
814 formate (pH 4.0), and solvent B was 80% acetonitrile in solvent A. Elution of the MU derivative  
815 was monitored by fluorescence detection (325 nm for excitation, and 380 nm for emission) and  
816 peak area used as a measure of activity. The enzymatic activity was calculated as the peak area of  
817 the product.

818 **Digestion of  $\alpha$ -DG with Exoglycosidases**

819 Exoglycosidase treatment was carried out as described previously (*Briggs et al., 2016; Salleh et*  
820 *al., 2006; Moracci et al., 2000*). *T. maritima*  $\beta$ -glucuronidase (*Salleh et al., 2006; Moracci et al.,*  
821 *2000*) (Bgus) and *S. solfataricus*  $\alpha$ -xylosidase (Xylsa), both bearing a His-tag were overexpressed  
822 in *E. coli*, and purified using TALON metal affinity resin as described and activity determined as  
823 described (*Salleh et al., 2006; Moracci et al., 2000*) with some modifications. Briefly, the cell  
824 pellet was resuspended in 20 mM HEPES buffer (pH 7.3), 150 mM NaCl, 0.1% NP-40 and  
825 sonicated. After centrifugation (30 minutes at 40,000 x g), the crude extract was incubated with  
826 Benzonase (Novagen) for 1 hour at room temperature and then heat-fractionated for 10 minutes at  
827 75°C. The supernatant was purified by using Talon metal affinity resin.

828 Samples to be digested by Bgus and Xylsa were exchanged into 150 mM sodium acetate (pH 5.5)  
829 solution and mixed with Bgus (0.45 U) and/or Xylsa (0.09 U), or no enzymes, and incubated  
830 overnight at 65°C. Samples were then run on SDS-PAGE, transferred to PVDF-FL (Millipore),  
831 and probed with anti- $\alpha$ -DG core antibody (AF6868) and anti- $\alpha$ -DG glycan antibody (IIH6).  
832 Enriched rabbit  $\alpha$ -DG (100  $\mu$ L of the 150 mM sodium acetate (pH 5.5) solution) was mixed with  
833 Bgus (0.45 U) and/or Xylsa (0.09 U), or no enzymes, and incubated overnight at 65°C. Samples  
834 were then run on SDS-PAGE, transferred to PVDF-FL (Millipore), and subjected to  
835 immunoblotting.

836 **Solid Phase Assay**

837 Solid phase assays were performed as described previously (*Michele et al., 2002; Goddeeris et*  
838 *al., 2013*). Briefly, WGA eluates were diluted 1:50 in TBS and coated on polystyrene ELISA  
839 microplates (Costar 3590) overnight at 4°C. Plates were washed in LBB and blocked for 2 hours  
840 in 3% BSA/LBB at RT. The wells were washed with 1% BSA/LBB and incubated for 1 hour with

841 L9393 (1:5,000 dilution) in 3% BSA/LBB followed by incubation with Horseradish Peroxidase  
842 (HRP)-conjugated anti-rabbit IgG (Invitrogen, 1:5,000 dilution) in 3% BSA/LBB for 30 minutes.  
843 Plates were developed with o-phenylenediamine dihydrochloride and H<sub>2</sub>O<sub>2</sub>, and reactions were  
844 stopped with 2 N H<sub>2</sub>SO<sub>4</sub>. Absorbance per well was read at 490 nm by a microplate reader.

845 **Statistics**

846 The included Shimadzu post-run software was used to analyze POMK, LARGE, and B4GAT1  
847 activity in fibroblasts and mouse skeletal muscle, and the percent conversion to product was  
848 recorded. The means of three experimental replicates (biological replicates, where each replicate  
849 represents a different pair of tissue culture plates or animals, i.e. control and knockout) were  
850 calculated using Microsoft Excel, and the mean percent conversion to product for the WT or  
851 control sample (Control human fibroblasts or POMK<sup>LoxP/LoxP</sup> skeletal muscle, respectively)  
852 reaction was set to 1. Percent conversion of each experimental reaction was subsequently  
853 normalized to that of the control, and statistics on normalized values were performed using  
854 GraphPad Prism 8. For analysis of POMK and LARGE activity in fibroblasts and mouse skeletal  
855 muscle, Student's T-Test was used (two-sided). Differences were considered significant at a p-  
856 value less than 0.05. Graph images were also created using GraphPad Prism and the data in the  
857 present study are shown as the means +/- SD unless otherwise indicated. The number of sampled  
858 units, n, upon which we report statistics for *in vivo* data, is the single mouse (one mouse is n=1).  
859 For measure of POMK activity in HAP1 cells, the percent conversion from GGM-MU to GGM(P)-  
860 MU was first calculated using the included Shimadzu analysis software. The means plus standard  
861 deviations of the percent conversion to GGM(P)-MU for three experimental replicates was  
862 calculated using GraphPad Prism 8. One-way ANOVA with the Dunnett's Method for Multiple  
863 Comparisons was performed, and the data for the *POMK* KO HAP1 sample set as the control.

864 Differences were considered significant at a p-value less than 0.05. Graph images were created in  
865 GraphPad and show mean +/- SD.

866 To measure POMK activity in control and NH13-284 skeletal muscle, we only performed one  
867 experimental replicate due to the limited amount of sample available. To measure B4GAT1  
868 activity, two technical replicates were performed from skeletal muscle. Protein concentration from  
869 control and NH13-284 skeletal muscle was also measured using two technical replicates. The  
870 percent conversion to product for the B4GAT1 reaction was divided by the protein concentration,  
871 and the values for these two technical replicates graphed using GraphPad Prism 8. The graph  
872 reported is shown as the mean +/- SD.

873 For flow cytometry analyses, six experimental replicates were performed, and the mean  
874 fluorescence intensity (MFI) reported. Statistics were performed using the Student's unpaired T-  
875 test, two-sided in GraphPad Prism 8 and the values reported as mean +/- SD.

876 **NMR Spectroscopy**

877 1D  $^1\text{H}$  NMR spectra of the core M3 trisaccharides GGM-MU and GGMP-MU in the absence and  
878 presence of POMK or LARGE were acquired at 25°C on a Bruker Avance II 800 MHz NMR  
879 spectrometer equipped with a sensitive cryoprobe by using a 50 ms  $T_2$  filter consisting of a train  
880 of spin-lock pulses to eliminate the broad resonances from the protein (*Mayer et al., 2001*). *Danio*  
881 *rerio* POMK titrations were performed in 25 mM Tris (pH 8.0), 180 mM NaCl, and 10 mM MgCl<sub>2</sub>  
882 in 98% D<sub>2</sub>O. LARGE titrations were performed in 20 mM HEPES, 150 mM NaCl, pH 7.3 in 90%  
883 H<sub>2</sub>O/10% D<sub>2</sub>O. The  $^{13}\text{C}$  and  $^1\text{H}$  resonances of the trisaccharides were reported previously  
884 (*Yoshida-Moriguchi et al., 2010*). The  $^1\text{H}$  chemical shifts are referenced to 2,2-dimethyl-2-  
885 silapentane-5-sulfonate. The NMR spectra were processed using NMRPipe (*Delaglio et al., 1995*)  
886 and analyzed using NMRView (*Johnson et al., 1994*). The glycan binding affinity to POMK and

887 LARGE was determined using glycan-observed NMR experiments as described previously  
888 (**Briggs et al., 2016**). For the resolved anomeric trisaccharide peak, the bound fraction was  
889 calculated by measuring the difference in the peak intensity in the absence (free form) and presence  
890 (bound form) of POMK or LARGE, and then dividing by the peak intensity of the free form. To  
891 obtain dissociation constant, the data were fitted to the standard quadratic equation using GraphPad  
892 Prism (GraphPad Software). The standard deviation from data fitting is reported.

893 **Mass Spectrometry**

894 In order to generate DG fusion proteins for MS analyses, HAP cells were grown in IMDM with  
895 10% FBS and 1% penicillin/streptomycin on p150 plates. When plates were 80% confluent, cells  
896 were washed twice with DPBS, media changed to serum-free IMDM with 1%  
897 penicillin/streptomycin (Invitrogen), and cells infected at high MOI (250-1000) of adenovirus  
898 expressing DG390TEVHis. Three days later, the media was harvested and stored at 4 degrees  
899 Celsius until samples were ready for MS analysis.

900 Reductive elimination. Glycans were reductively eliminated from DG390 proteins and purified on  
901 a 50WS8 Dowex column, and the purified glycans were subjected to permethylation and purified  
902 according to published methods (**Jang-Lee et al., 2006; Zhang et al., 2014**). Briefly, the freeze-  
903 dried DG390 sample was dissolved in 55 mg/mL potassium borohydride in 1 mL of a 0.1 M  
904 potassium hydroxide solution. The mixture was incubated for 18 hours at 45°C and quenched by  
905 adding five to six drops of acetic acid. The sample was loaded on the Dowex column and  
906 subsequently eluted with 5% acetic acid. The collected solution was concentrated and lyophilized,  
907 and excessive borates were removed with 10% methanolic acetic acid.

908 Permetylation. For the permethylation reaction, three to five pellets per sample of sodium  
909 hydroxide were crushed in 3 mL dry dimethyl sulfoxide. Methyl Iodine (500 mL) as well as the

910 resulting slurry (0.75 mL) were added to the sample. The mixture was agitated for 15 minutes and  
911 quenched by adding 2 mL ultrapure water with shaking. The glycans were extracted with  
912 chloroform (2 mL) and washed twice with ultrapure water. Chloroform was removed under a  
913 stream of nitrogen. The permethylated glycans were loaded on a C18 Sep-pak column, washed  
914 with 5 mL ultrapure water and successively eluted with 3 mL each of 15, 35, 50 and 75% aq.  
915 acetonitrile. The solutions were collected and lyophilized.

916 Mass spectrometry. A Bruker Autoflex III MALDI TOF/TOF was used for acquisition of all  
917 MALDI MS data. An in-house made BSA digest was used to calibrate the MS mode. 3,4-  
918 diaminobenzophenone was used as the matrix. Permethylated samples were dissolved in 10 mL of  
919 methanol, and 1  $\mu$ L of this solution was premixed with 1  $\mu$ L matrix. 1  $\mu$ L of this mixture was  
920 spotted on the plate.

921 **Data Availability**

922 All data generated or analyzed during this study are included in this published article.

923 **Acknowledgements**

924 The BRC/ MRC Centre for Neuromuscular Diseases Biobank is acknowledged for providing  
925 patients' serum and biopsy samples. The Muscular Dystrophy UK support to the GOSH  
926 Neuromuscular Centre is also gratefully acknowledged. We wish to thank Norma Sinclair,  
927 Patricia Yarolem, JoAnn Schwarting and Rongbin Guan for their technical expertise in  
928 generating transgenic mice.

929

930 **Authors' Contributions**

931 ASW and KPC designed experiments and wrote the manuscript. ASW, HO, SJ, TY, TY, DV,  
932 JMH, MC, ST, MEA, LY, MD, SOL, and SJP performed experiments. AM, ST, JX, JED, and  
933 FM provided critical information and materials regarding the patient. FM was involved in  
934 meaningful discussions regarding the manuscript. All authors contributed to and gave feedback  
935 on the manuscript.

936

937 **Competing Interests**

938 The authors declare no competing financial interests. Correspondence and requests for materials  
939 should be addressed to K.P.C. ([kevin-campbell@uiowa.edu](mailto:kevin-campbell@uiowa.edu)).

940

941 **Funding**

942 This work was supported in part by a Paul D. Wellstone Muscular Dystrophy Specialized  
943 Research Center grant (1U54NS053672 to KPC). S. T and F.M. are supported by the National  
944 Institute for Health Research Biomedical Research Centre at Great Ormond Street Hospital for  
945 Children NHS Foundation Trust and University College London. A.S.W. is a student in the

946 University of Iowa Medical Scientist Training Program, which is funded by Medical Scientist  
947 Training Program Grant by the National Institute of General Medical Sciences (NIGMS) 5 T32  
948 GM007337. Transgenic mice were generated at the University of Iowa Genome Editing Core  
949 Facility directed by William Paradee, PhD and supported in part by grants from the NIH and  
950 from the Roy J. and Lucille A. Carver College of Medicine. KPC is an investigator of the  
951 Howard Hughes Medical Institute.

952

953 **References**

954 Anderson, R. D., Haskell, R. E., Xia, H., Roessler, B. J., & Davidson, B. L. A simple method for  
955 the rapid generation of recombinant adenovirus vectors. *Gene Ther.* **7**, 1034-1038 (2000).  
956 DOI: 10.1038/sj.gt.3301197, PMID: 10871752

957 Barresi, R., Michele, D.E., Kanagawa, M., Harper, H.A., Dovico, S.A., Satz, J.S., Moore, S.A.,  
958 Zhang, W., Schachter, H., Dumanski, J.P., Cohn, R.D., Nishino, I., Campbell, K.P. LARGE  
959 can functionally bypass alpha-dystroglycan glycosylation defects in distinct congenital  
960 muscular dystrophies. *Nat Med.* **10**, 696-703 (2004). DOI: 10.1038/nm1059, PMID:  
961 15184894

962 Briggs, D. C., Yoshida-Moriguchi, T., Zheng, T., Venzke, D., Anderson, M.E., Strazzulli, A.,  
963 Moracci, M., Yu, L., Hohenester, E., Campbell, K.P. Structural basis of laminin binding to  
964 the LARGE glycans on dystroglycan. *Nat Chem Biol.* **12**, 810-814 (2016). DOI:  
965 10.1038/nchembio.2146, PMID: 27526028

966 Brüning, J. C., Michael, M.D., Winnay, J.N., Hayashi, T., Hörsch, D., Accili, D., Goodyear, L.J.,  
967 Kahn, C.R. A muscle-specific insulin receptor knockout exhibits features of the metabolic

968 syndrome of NIDDM without altering glucose tolerance. *Mol Cell.* **5**, 559-569 (1998). DOI:  
969 10.1016/s1097-2765(00)80155-0, PMID: 9844629

970 Cohn, R.D., Henry, M.D., Michele, D.E., Barresi, R., Saito, F., Moore, S.A., Flanagan, J.D.,  
971 Skwarchuk, M.W., Robbins, M.E., Mendell, J.R., Williamson, R.A., Campbell, K.P.  
972 Disruption of DAG1 in differentiated skeletal muscle reveals a role for dystroglycan in  
973 muscle regeneration. *Cell.* **110**, 639-648 (2002). DOI: 10.1016/s0092-8674(02)00907-8,  
974 PMID: 12230980

975 Delaglio, F., Grzesiek, S., Vuister, G.W., Zhu, G., Pfeifer, J., Bax, A. NMRPipe: a  
976 multidimensional spectral processing system based on UNIX pipes. *J. Biomol. NMR.* **6**, 277-  
977 293 (1995). DOI: 10.1007/BF00197809, PMID: 8520220

978 Di Costanzo, S. Balasubramanian, A., Pond, H.L., Rozkalne, A., Pantaleoni, C., Saredi, S.,  
979 Gupta, V.A., Sunu, C.M., Yu, T.W., Kang, P.B., Salih, M.A., Mora, M., Gussoni, E., Walsh,  
980 C.A., Manzini, M.C. POMK mutations disrupt muscle development leading to a spectrum of  
981 neuromuscular presentations. *Hum Mol Genet.* **23**, 5781-5792 (2014). DOI:  
982 10.1093/hmg/ddu296, PMID: 24925318

983 Ervasti, J. M. & Campbell, K. P. Membrane organization of the dystrophin-glycoprotein  
984 complex. *Cell.* **66**, 1121-1131 (1991). DOI: 10.1016/0092-8674(91)90035-w, PMID:  
985 1913804

986 Gerin, I., Ury, B., Breloy, I., Bouchet-Seraphin, C., Bolsée, J., Halbout, M., Graff, J.,  
987 Vertommen, D., Muccioli, G.G., Seta, N., Cuisset, J.-M., Dabaj, I., Quijano-Roy, S., Grahn,  
988 A., Schaftingen, E.V., Bommer, G.T. ISPD produces CDP-ribitol used by FKTN and FKRP  
989 to transfer ribitol phosphate onto  $\alpha$ -dystroglycan. *Nat. Commun.* **7**, 11534 (2016). DOI:  
990 10.1038/ncomms11534, PMID: 27194101

991 Goddeeris, M. M., Wu, B., Venzke, D., Yoshida-Moriguchi, T., Saito, F., Matsumura, K.,  
992 Moore, S.A., Campbell, K.P. LARGE glycans on dystroglycan function as a tunable matrix  
993 scaffold to prevent dystrophy. *Nature*. **503**, 136-140 (2013). DOI: 10.1038/nature12605,  
994 PMID: 24132234

995 Han, R., Kanagawa, M., Yoshida-Moriguchi, T., Rader, E.P., Ng, R.A., Michele, D.E.,  
996 Muirhead, D.E., Kunz, S., Moore, S.A., Iannaccone, S.T., Miyake K., McNeil, P.L., Mayer,  
997 U., Oldstone, M.B.A., Faulkner, J.A., Campbell, K.P. Basal lamina strengthens cell  
998 membrane integrity via the laminin G domain-binding motif of  $\alpha$ -dystroglycan. *Proceedings*  
999 of the National Academy of Sciences. **106**, 12573-12579 (2009). DOI:  
1000 10.1073/pnas.0906545106, PMID: 19633189

1001 Hara, Y., Balci-Hayta, B., Yoshida-Moriguchi, T., Kanagawa, M., Beltrán-Valero de Bernabé.,  
1002 Gündesli, H., Willer, T., Satz, J.S., Crawford, R.W., Burden, S.J., Kunz, S., Oldstone,  
1003 M.B.A., Accardi, A., Talim, B., Muntoni, F., Topaloğlu, H., Dinçer, P., Campbell, K.P. A  
1004 dystroglycan mutation associated with limb-girdle muscular dystrophy. *N Engl J Med*. **364**,  
1005 939-946 (2011). DOI: 10.1056/NEJMoa1006939, PMID: 21388311

1006 Hara, Y., Kanagawa, M., Kunz, S., Yoshida-Moriguchi, T., Satz, J.S., Kobayashi, Y.M., Zhu, Z.,  
1007 Burden, S.J., Oldstone, M.B.A., Campbell, K.P. Like-acetylglucosaminyltransferase  
1008 (LARGE)-dependent modification of dystroglycan at Thr-317/319 is required for laminin  
1009 binding and arenavirus infection. *Proc Natl Acad Sci U S A*. **108**, 17426-17431 (2011). DOI:  
1010 10.1073/pnas.1114836108, PMID: 21987822

1011 Hohenester, E. Laminin G-like domains: dystroglycan-specific lectins. *Current Opinion in*  
1012 *Structural Biology*. **56**, 56-63 (2019). DOI: 10.1016/j.sbi.2018.11.007, PMID: 30530204

1013 Hohenester, E., Tisi, D., Talts, J. F., & Timpl, R. The crystal structure of a laminin G-like  
1014 module reveals the molecular basis of  $\alpha$ -dystroglycan binding to laminins, perlecan, and  
1015 agrin. *Mol Cell.* **4**, 783-792 (1999). DOI: 10.1016/s1097-2765(00)80388-3, PMID: 10619025

1016 Hudson, BG. Tryggvason, K., Sundaramoorthy, M., Neilson, E.G. Alport's syndrome,  
1017 Goodpasture's syndrome, and type IV collagen. *N Engl J Med.* **348**, 2543-2556 (2003). DOI:  
1018 10.1056/NEJMra022296, PMID: 12815141

1019 Inamori, K., Yoshida-Moriguchi, T., Hara, Y., Anderson, M.E., Yu, L., Campbell, K.P.  
1020 Dystroglycan function requires xylosyl- and glucuronyltransferase activities of LARGE.  
1021 *Science.* **335**, 93-96 (2012). DOI: 10.1126/science.1214115, PMID: 22223806

1022 Jae, L.T., Raaben, M., Riemersma, M., van Beusekom, E., Blomen, V.A., Velds, A., Kerkhoven,  
1023 R.M., Carette, J.E., Topaloglu, H., Meinecke, P., Wessels, M.W., Lefeber, D.J., Whelan,  
1024 S.P., van Bokhoven, H., Brummelkamp, T.R. Deciphering the glycosylome of  
1025 dystroglycanopathies using haploid screens for lassa virus entry. *Science.* **340**, 479-483  
1026 (2013). DOI: 10.1126/science.1233675, PMID: 23519211

1027 Jang-Lee, J., North, S.J., Sutton-Smith, M., Goldberg, D., Panico, M., Morris, H., Haslam, S.,  
1028 Dell, A. Glycomic profiling of cells and tissues by mass spectrometry: fingerprinting and  
1029 sequencing methodologies. *Meth. Enzymol.* **415**, 59–86 (2006). DOI: 10.1016/S0076-  
1030 6879(06)15005-3, PMID: 17116468

1031 Johnson, B. A., & Blevins, R. A. NMR View: A computer program for the visualization and  
1032 analysis of NMR data. *J. Biomol. NMR.* **4**, 603-614 (1994). DOI: 10.1007/BF00404272,  
1033 PMID: 22911360

1034 Kanagawa, M., Kobayashi, K., Tajiri, M., Manya, H., Kuga, A., Yamaguchi, Y., Manya-  
1035 Akasaka, K., Furukawa, J.-I., Mizuno, M., Kawakami, H., Shinohara, Y., Wada, Y., Endo,

1036 T., Toda, T. Identification of a Post-translational Modification with Ribitol-Phosphate and Its  
1037 Defect in Muscular Dystrophy. *Cell Reports* **9**, 2209-2223 (2016). DOI:  
1038 10.1016/j.celrep.2016.02.017, PMID: 26923585

1039 Kanagawa, M., Nishimoto, A., Chiyonobu, T., Takeda, S., Miyagoe-Suzuki, Y., Wang, F.,  
1040 Fujikake, N., Taniguchi, M., Lu, Zhongpeng, L., Tachikawa, M., Nagai, Y., Tashiro, F.,  
1041 Miyazaki, J.-I., Tajima, Y., Takeda, S., Endo, T., Kobayashi, K., Campbell, K.P., Toda, T.  
1042 Residual Laminin-Binding Activity and Enhanced Dystroglycan Glycosylation by LARGE in  
1043 Novel Model Mice to Dystroglycanopathy. *Hum Mol Genet.* **18**, 621-631 (2009). DOI:  
1044 10.1093/hmg/ddn387, PMID: 19017726

1045 Kanagawa, M., Saito, F., Kunz, S., Yoshida-Moriguchi, T., Barresi, T., Kobayashi, Y.M.,  
1046 Muschler, J., Dumanski, J.P., Michele, D.E., Oldstone, M.B.A., Campbell, K.P. Molecular  
1047 recognition by LARGE is essential for expression of functional dystroglycan. *Cell.* **117**, 953-  
1048 964 (2004). DOI: 10.1016/j.cell.2004.06.003, PMID: 15210115

1049 Keller, C., Hansen, M. S., Coffin, C. M., & Capecchi, M. R. Pax3:Fkhr interferes with  
1050 embryonic Pax3 and Pax7 function: implications for alveolar rhabdomyosarcoma cell of  
1051 origin. *Genes Dev.* **18**, 2608-2013 (2004). DOI: 10.1101/gad.1243904, PMID: 15520281

1052 Kunz, S., Sevilla, N., McGavern, D. B., Campbell, K. P., & Oldstone, M. B. Molecular analysis  
1053 of the interaction of LCMV with its cellular receptor  $\alpha$ -dystroglycan. *J Cell Biol.* **155**, 301-  
1054 310 (2001). DOI: 10.1083/jcb.200104103, PMID: 11604425

1055 Mayer, M., & Meyer, B. Group epitope mapping by saturation transfer difference NMR to  
1056 identify segments of a ligand in direct contact with a protein receptor. *J. Am. Chem. Soc.* **123**,  
1057 6108-6117 (2001). DOI: 10.1021/ja0100120, PMID: 11414845

1058 Michele, D. E., Barresi, R., Kanagawa, M., Saito, F., Cohn, R.D., Satz, J.S., Dollar, J., Nishino,  
1059 I., Kelley, R.I., Somer, H., Straub, V., Mathews, K.D., Moore, S.A., Campbell, K.P. Post-  
1060 translational disruption of dystroglycan-ligand interactions in congenital muscular  
1061 dystrophies. *Nature*. **418**, 417-422 (2002). DOI: 10.1038/nature00837, PMID: 12140558  
1062 Moracci, M., Ponzano, B.C., Trincone, A., Fusco, S., De Rosa, M., van Der Oost, J., Swensen,  
1063 C.W., Charlebois, R.L., Rossi, M. Identification and molecular characterization of the first  
1064  $\alpha$ -xylosidase from an archaeon. *J. Biol. Chem.* **275**, 22082-22089 (2000). DOI:  
1065 10.1074/jbc.M910392199, PMID: 10801892  
1066 Ohtsubo, K., & Marth, J. D. Glycosylation in cellular mechanisms of health and disease. *Cell*.  
1067 **126**, 855-867 (2006). DOI: 10.1016/j.cell.2006.08.019, PMID: 16959566  
1068 Pinkert, C. A. Ed., *Transgenic Animal Technology: A Laboratory Handbook* (Academic Press,  
1069 ed. 2, 2002), pp. 20-31.  
1070 Rader, E.P, Turk R., Willer T., Beltran D., Inamori K., Peterson, .T.A, Engle, J., Prouty S.,  
1071 Matsumura, K., Saito, F., Anderson M.E., Campbell, K.P. Role of dystroglycan in limiting  
1072 contraction-induced injury to the sarcomeric cytoskeleton of mature skeletal muscle. *Proc.*  
1073 *Natl. Acad. Sci. U.S.A.* **113**, 10992–10997 (2016). DOI: 10.1073/pnas.1605265113, PMID:  
1074 27625424  
1075 Riemersma, M., Froese, S.D., van Tol, W., Engelke, U.F., Kopec, J., van Scherpenzeel, M.,  
1076 Ashikov, A., Krojer, T., von Delft, F., Tessari, M., Buczkowska, A., Swiezewska, E., Jae,  
1077 L.T., Brummelkamp, T.R., Manya, H., Endo, T., van Bokhoven, H., Yue, W.W., Lefeber,  
1078 D.J. Human ISPD Is a Cytidyltransferase Required for Dystroglycan O-Mannosylation.  
1079 *Chem Biol.* **12**, 1643-1652 (2015). DOI: 10.1016/j.chembiol.2015.10.014, PMID: 26687144

1080 Rowe, R.G. & Weiss, S.J. Breaching the basement membrane: who, when and how? *Trends Cell  
1081 Biol.* **18**, 560-74 (2008). DOI: 10.1016/j.tcb.2008.08.007, PMID: 18848450

1082 Salleh, H. M., Mullegger, J., Reid, S.P., Chan, W.Y., Hwang, J., Warren, R.A.J., Withers, S.G.  
1083 Cloning and characterization of *Thermotoga maritima*  $\beta$ -glucuronidase. *Carbohydr. Res.* **341**,  
1084 49-59 (2006). DOI: 10.1016/j.carres.2005.10.005, PMID: 16303119

1085 von Renesse, A., Petkova, M.V., Lutzkendorf, S., Heinemeyer, J., Gill, E., Hübner, C., Moers,  
1086 A.V., Stenzel, W., Schuelke, M. POMK mutation in a family with congenital muscular  
1087 dystrophy with merosin deficiency, hypomyelination, mild hearing deficit and intellectual  
1088 disability. *J Med Genet.* **51**, 275-282 (2014). DOI: 10.1136/jmedgenet-2013-102236, PMID:  
1089 24556084

1090 Willer, T., Inamori, K., Venzke, D., Harvey, C., Morgensen, G., Hara, Y., Beltran Valero de  
1091 Bernabe, D., Yu, L., Wright, K.M., Campbell, K.P. The glucuronyltransferase B4GAT1 is  
1092 required for initiation of LARGE-mediated  $\alpha$ -dystroglycan functional glycosylation. *eLife.* **3**,  
1093 e03941 (2014). DOI: 10.7554/eLife.03941, PMID: 25279699

1094 Willer, T., Lee, H., Lommel, M., Yoshida-Moriguchi, T., Beltran Valero de Bernabe, D.,  
1095 Venzke, D., Cirak, S., Schachter, H., Vajsar, J., Voit, T., Muntoni, F., Loder, A.S., Dobyns,  
1096 W.B., Winder, T.L., Strahl, S., Mathews, K.D., Nelson, S.F., Moore, S.A., Campbell, K.P.  
1097 ISPD loss-of-function mutations disrupt dystroglycan O-mannosylation and cause Walker-  
1098 Warburg syndrome. *Nat Genet.* **44**, 575-580 (2012). DOI: 10.1038/ng.2252, PMID:  
1099 22522420

1100 Yoshida-Moriguchi, T. & Campbell, K. P. Matriglycan: a novel polysaccharide that links  
1101 dystroglycan to the basement membrane. *Glycobiology.* **25**, 702-713 (2015). DOI:  
1102 10.1093/glycob/cwv021, PMID: 25882296

1103 Yoshida-Moriguchi, T., Willer, T., Anderson, M.E., Venzke, D., Whyte, T., Muntoni, F., Lee,  
1104 H., Nelson, S.F., Yu, L., Campbell, K.P. SGK196 is a glycosylation-specific *O*-mannose  
1105 kinase required for dystroglycan function. *Science*. **341**, 896-899 (2013). DOI:  
1106 10.1126/science.1239951, PMID: 23929950

1107 Yoshida-Moriguchi, T., Yu, L., Stalnaker, S.H., Davis, S., Kunz, S., Madson, M., Oldstone,  
1108 M.B.A., Schachter, H., Wells, L., Cambell, K.P. *O*-mannosyl phosphorylation of  $\alpha$ -  
1109 dystroglycan is required for laminin binding. *Science*. **327**, 88-92 (2010). DOI:  
1110 10.1126/science.1180512, PMID: 20044576

1111 Zhang, H., Zhu, F., Yang, T., Ding, L., Zhou, M., Li, J., Haslam, S.M., Dell, A., Erlandsen, H.,  
1112 Wu, H. The highly conserved domain of unknown function 1792 has a distinct  
1113 glycosyltransferase fold. *Nat Commun*. **5**, 4339 (2014). DOI: 10.1038/ncomms5339, PMID:  
1114 25023666

1115 Zhu, Q., Venzke, D., Walimbe, A.S., Anderson, M.E., Fu, Q., Kinch, L.N., Wang, W., Chen, X.,  
1116 Grishin, N.V., Huang, N., Yu, L., Dixon, J.E., Campbell, K.P., Xiao, J. Structure of protein  
1117 *O*-mannose kinase reveals a unique active site architecture. *eLife*. **5**, e22238 (2016). DOI:  
1118 10.7554/eLife.22238, PMID: 27879205

1119 **SUPPLEMENTARY TEXT**

1120 We transduced *POMK/DG* KO HAP1 and *POMK* KO HAP1 cells with an adenovirus expressing  
1121 wild-type DG (Ad-DG). We observed a return of the laminin binding at 90-100 kDa in *POMK/DG*  
1122 KO HAP1 cells (**Figure 7-Figure Supplement 4A**) and an increase in the corresponding IIH6  
1123 immunoreactivity and laminin binding in *POMK* KO HAP1 cells (**Figure 7-Figure Supplement**  
1124 **6A, 6B, 6C**), further indicating that the glycoprotein responsible is  $\alpha$ -DG.

1125

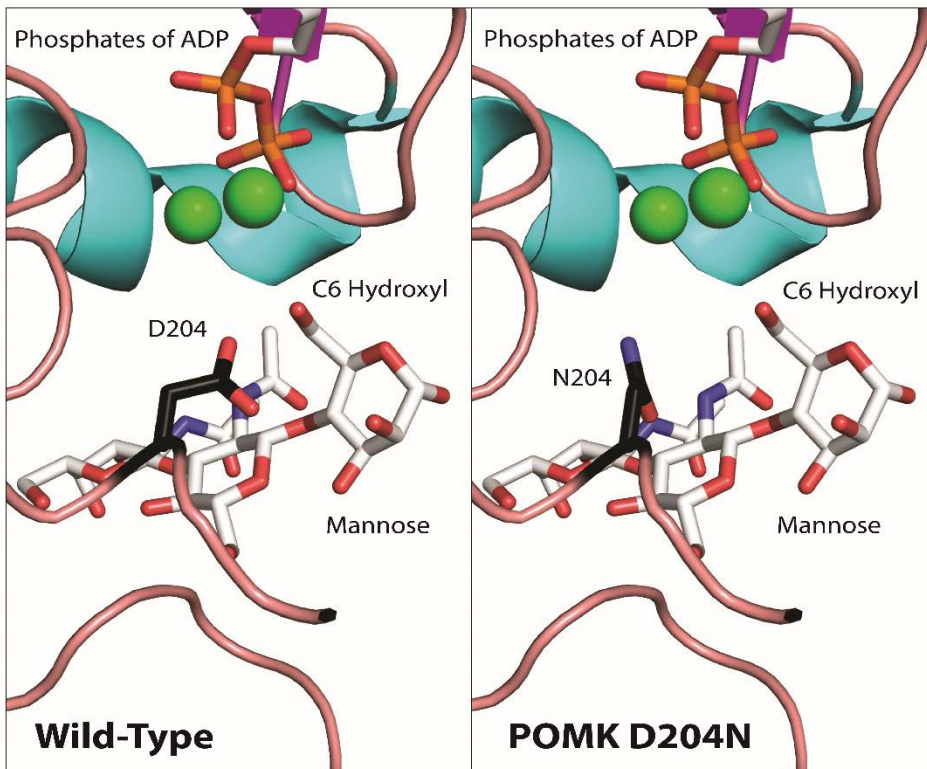
1126 The binding of a xylose-glucuronic acid repeat of matriglycan to the LG-domains of ECM ligands  
1127 is calcium-dependent (*Yoshida-Moriguchi et al., 2015; Hohenester, 2019; Briggs et al., 2016*).  
1128 To test if the binding of the non-extended matriglycan is similarly calcium-dependent, we  
1129 performed laminin overlays in the presence of 10 mM EDTA (**Figure 7-Figure Supplement 6D,**  
1130 **6E**). In both WT and *POMK* KO HAP1 cells, there was a complete absence of laminin binding in  
1131 the presence of EDTA, indicating that laminin binding at 90-100 kDa is calcium-dependent and  
1132 the glycan responsible is composed of xylose-glucuronic acid repeats.

1133

1134 Given the higher affinity of POMK for the unphosphorylated core M3 compared to the  
1135 phosphorylated form (**Figure 8C; Figure 8-Figure Supplement 1A**), it is possible that POMK  
1136 D204N, which is catalytically inactive, binds to GGM and increases the amount of core M3-  
1137 modified  $\alpha$ -DG in the ER, thereby reducing the amount entering the Golgi. With a reduction in the  
1138 amount of core M3-modified  $\alpha$ -DG entering the Golgi, FKTN may be able to better modify GalNac  
1139 of the unphosphorylated core M3, thus enabling the formation of the matriglycan which enables  
1140 laminin binding at 90-100 kDa in the patient's skeletal muscle. In *POMK* KO HAP1 cells alone,  
1141 the non-extended matriglycan represents the amount formed when no POMK is present and  
1142 transport of core M3-modified  $\alpha$ -DG to the Golgi is not reduced. In support of this hypothesis,  
1143 overexpression of POMK D204N in *POMK* KO HAP1 cells at a higher multiplicity of infection  
1144 (MOI) of 10 leads to higher MW forms of matriglycan despite the catalytic inactivity of POMK  
1145 D204N *in vitro* (**Figure 7-Figure Supplement 6F**). The higher MW of this form of matriglycan  
1146 resembles that of the POMK D204N skeletal muscle. Alternatively, it is possible that POMK  
1147 D204N remains attached to the unphosphorylated core M3 and this binary complex of POMK  
1148 D204N and  $\alpha$ -DG moves to the Golgi, where it can form a ternary complex with FKTN. The  
1149 ternary complex composed of FKTN, POMK D204N, and  $\alpha$ -DG enables FKTN to more efficiently  
1150 elongate the core M3 leading to formation of the non-extended matriglycan. Further studies will  
1151 be needed to determine the precise mechanism.

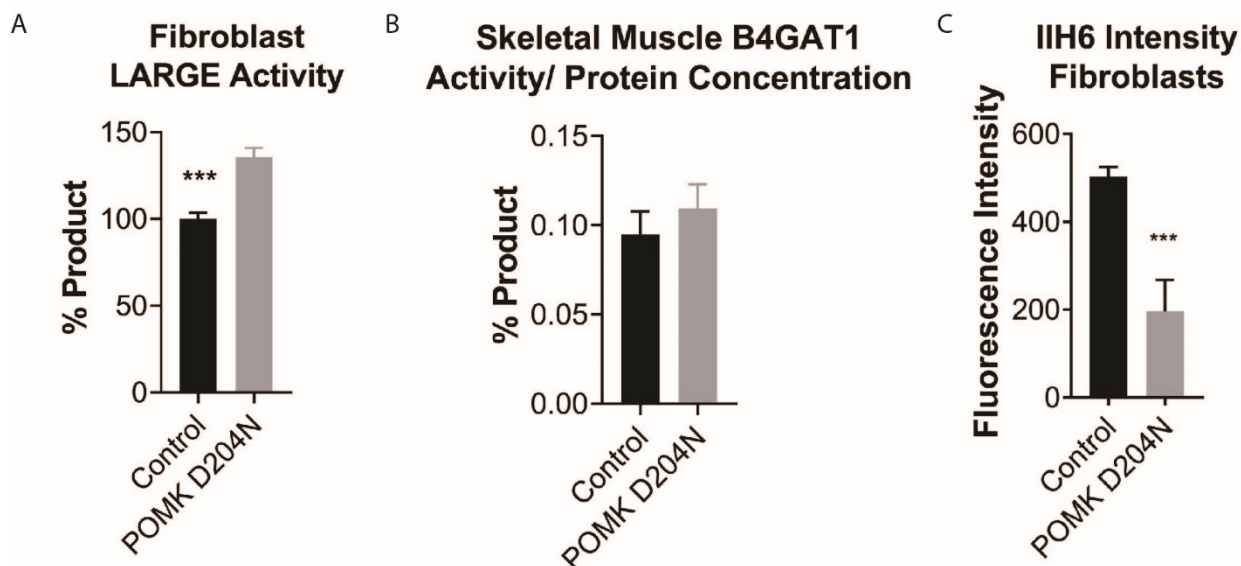
1152 **Supplementary Figures**

1153



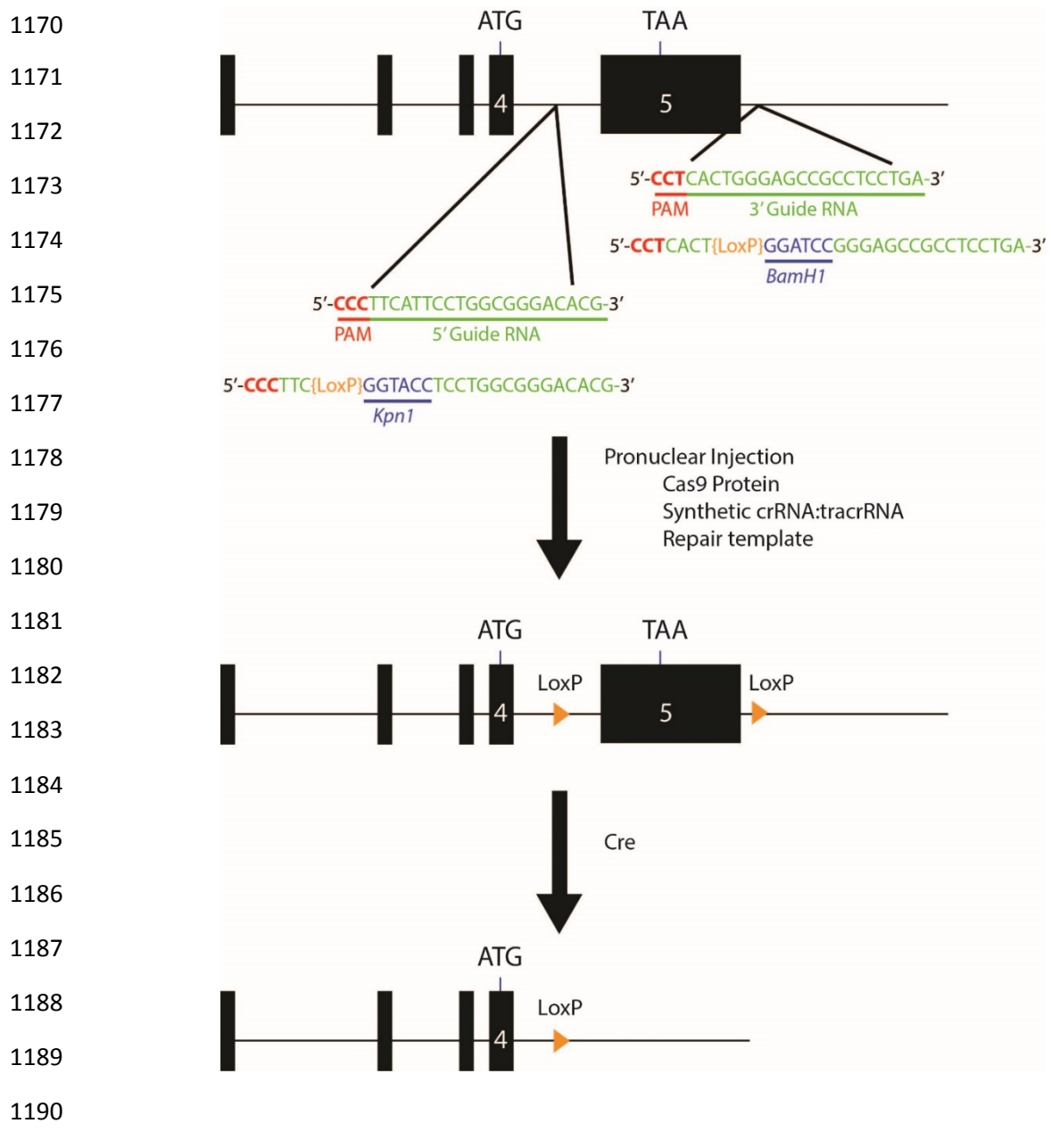
1154

1155 **Figure 2 - Figure Supplement 1.** Structural Modeling of POMK D204N Mutation. This figure  
1156 shows structural modeling of wild-type POMK and the POMK D204N mutation using human  
1157 POMK protein sequence numbering, based on the crystal structure of Zebrafish POMK. The  
1158 green spheres indicate manganese ions. The phosphorous, oxygen, nitrogen, and carbon atoms  
1159 are colored in orange, red, blue, and white, respectively. The D204 and N204 carbon atoms are  
1160 colored dark. The gamma phosphate of ATP is not shown.



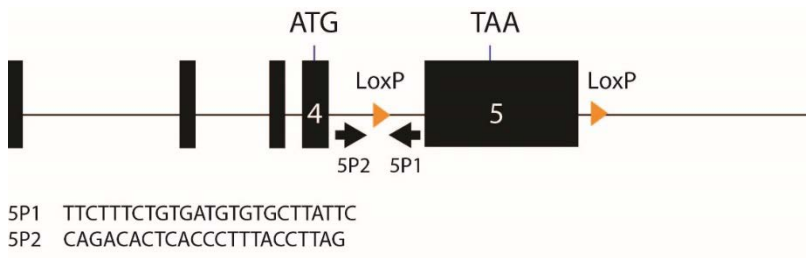
1161

1162 **Figure 2 - Figure Supplement 2.** Supplemental Analysis of POMK D204N Fibroblasts and  
1163 Muscle. **A**, LARGE activity in control human fibroblasts and fibroblasts from patient NH13-284  
1164 (POMK D204N). Triple asterisks indicate  $p$ -value $<0.001$  using Student's unpaired t-test (three  
1165 replicates). **B**, B4GAT1 activity (normalized to protein concentration) from control human  
1166 skeletal muscle and POMK D204N muscle. **C**, Mean fluorescence intensity of control human  
1167 fibroblasts and POMK D204N fibroblasts. Flow cytometry analyses were performed using an  
1168 antibody against matriglycan (IIH6). Triple asterisks indicate statistical significance with  $p$ -  
1169 value $<0.001$  using Student's unpaired t-test (three replicates).



1192 **Figure 3 - Figure Supplement 1.** Schematic for Generation of Floxed Alleles of *POMK*. Map of  
1193 5' and 3' LoxP sites (orange). LoxP sites flanking exon 5 of *POMK* (large black box), which  
1194 encodes the majority of the kinase domain of *POMK*, were inserted using CRISPR/Cas9. Cre-  
1195 mediated recombination of the floxed allele of *POMK* is predicted to lead to a loss of exon 5.

1196 A



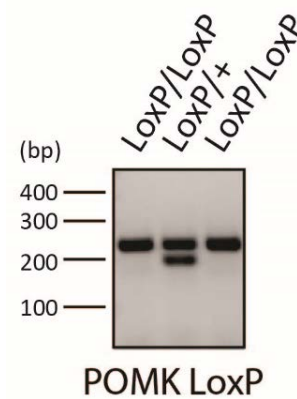
1197

1198

1199

1200 **Figure 3 - Figure Supplement 2.** Results of *POMK*<sup>LoxP</sup> Genotyping. **A**, Genotyping Strategy for  
1201 floxed *POMK* Allele. PCR Primers were designed to flank the 5' LoxP site. **B**, the *wild-type*  
1202 allele is 197 bp, while the *LoxP* allele is 235 base pairs.

B



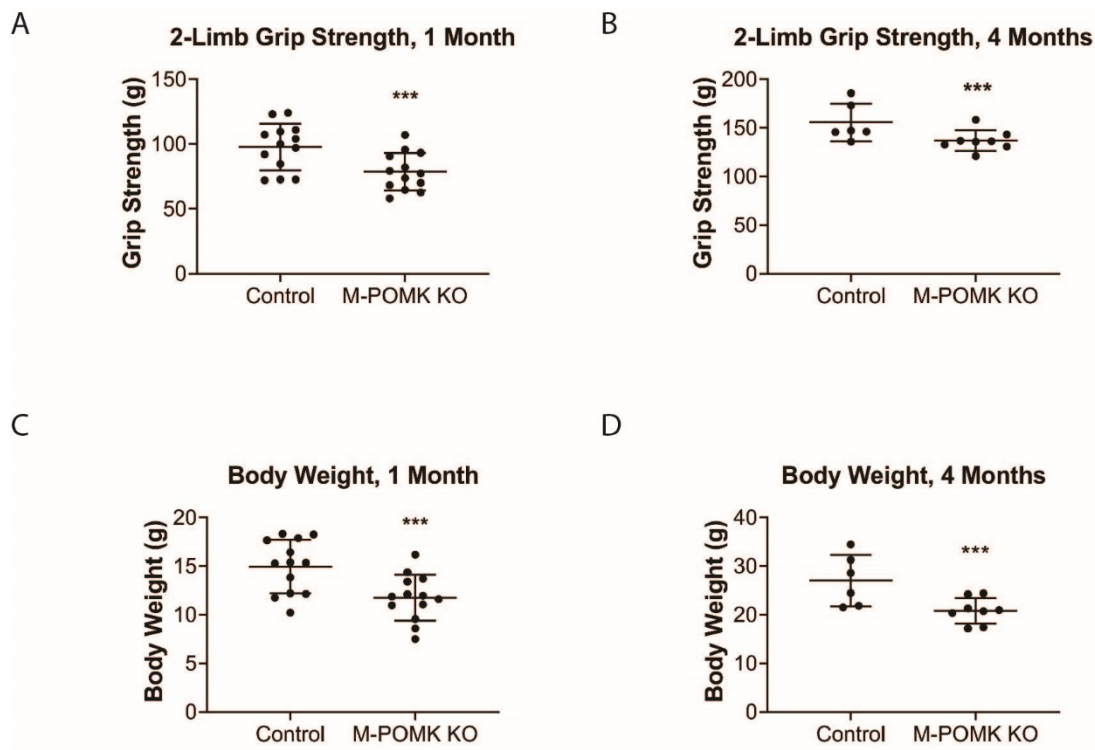
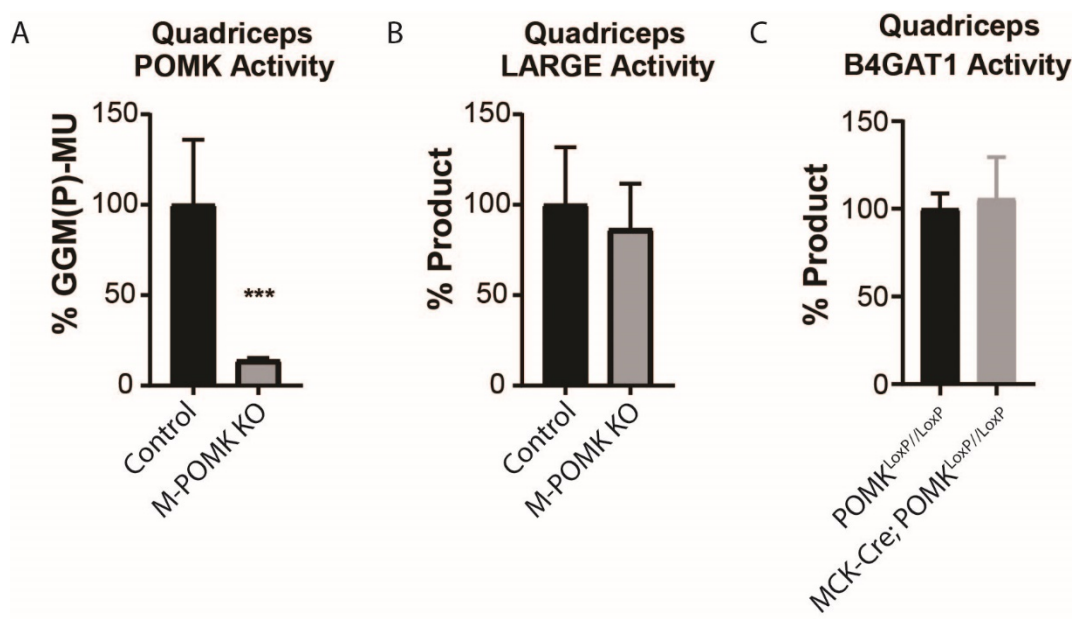


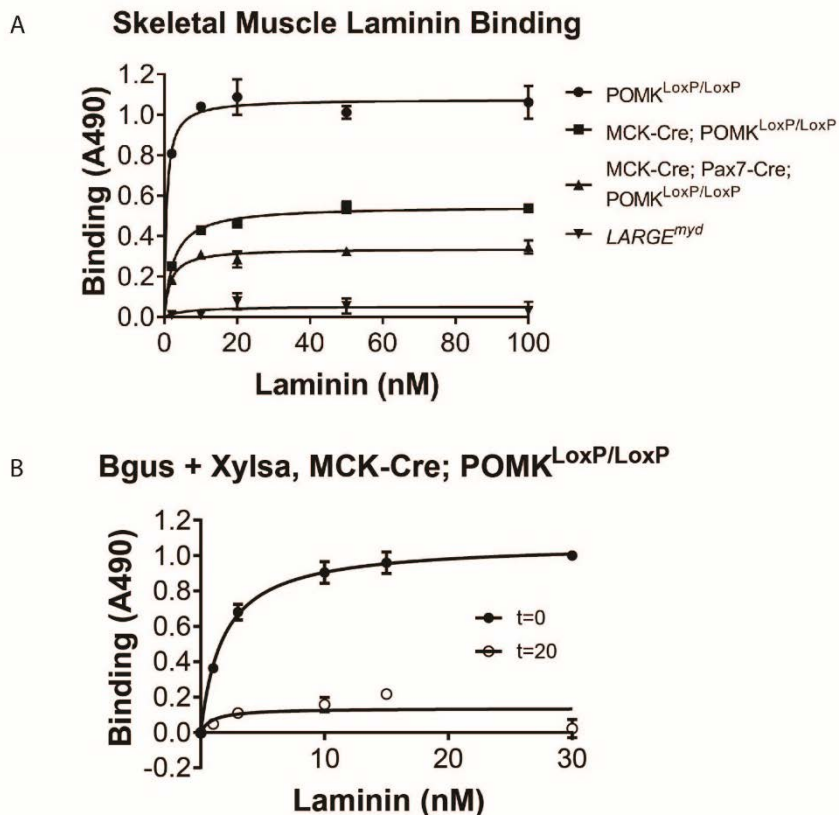
**Figure 3 - Figure Supplement 3.** Muscle-Specific POMK Knockout Mice Have Reduced Grip Strength and Body Weight. **A, B**, 2-limb grip strength of 1-month old (**A**) and 4-month old (**B**)  $\text{POMK}^{\text{LoxP}/\text{LoxP}}$  (Control) and MCK-Cre; Pax7-Cre;  $\text{POMK}^{\text{LoxP}/\text{LoxP}}$  (M-POMK KO) mice. **C, D**, Body weights of 1-month old (**C**) and 4-month old (**D**) Control and M-POMK KO mice. Triple asterisks:  $p$ -value  $< 0.05$  using Student's unpaired t-test.



1209

1210 **Figure 3 - Figure Supplement 4.** Supplemental Biochemical Analysis of POMK Null Skeletal  
1211 Muscle. **A, B**, POMK (**A**) and LARGE (**B**) activity of M-POMK KO and POMK<sup>LoxP/LoxP</sup>  
1212 (Control) quadriceps muscle extracts (three replicates). Asterisks indicate P-value=0.01 using  
1213 Student's unpaired t-test. **C**, B4GAT1 activity in MCK-Cre; POMK<sup>LoxP/LoxP</sup> and control  
1214 quadriceps muscle extracts (three replicates).

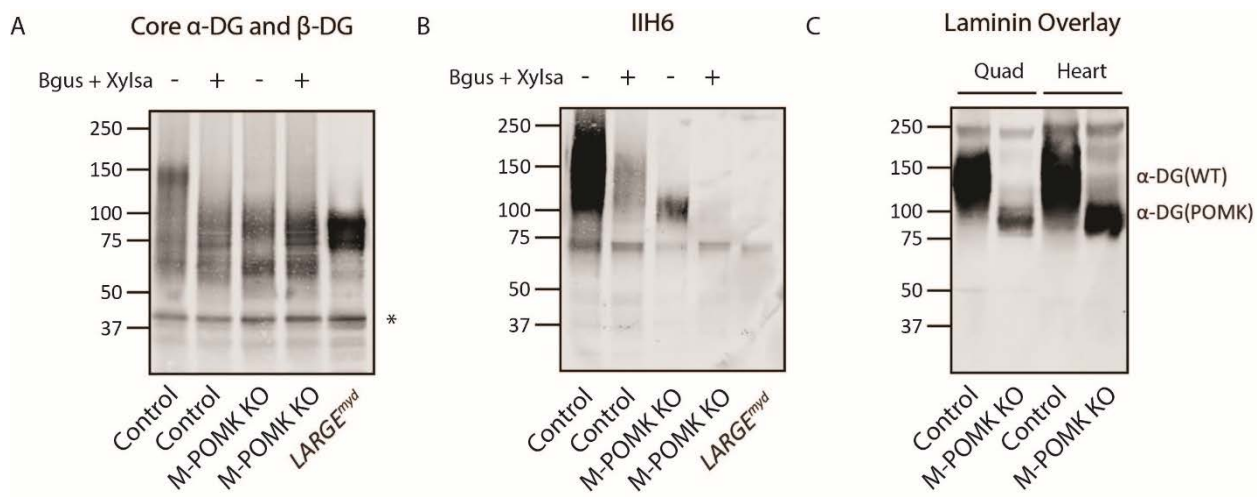
1215



1216

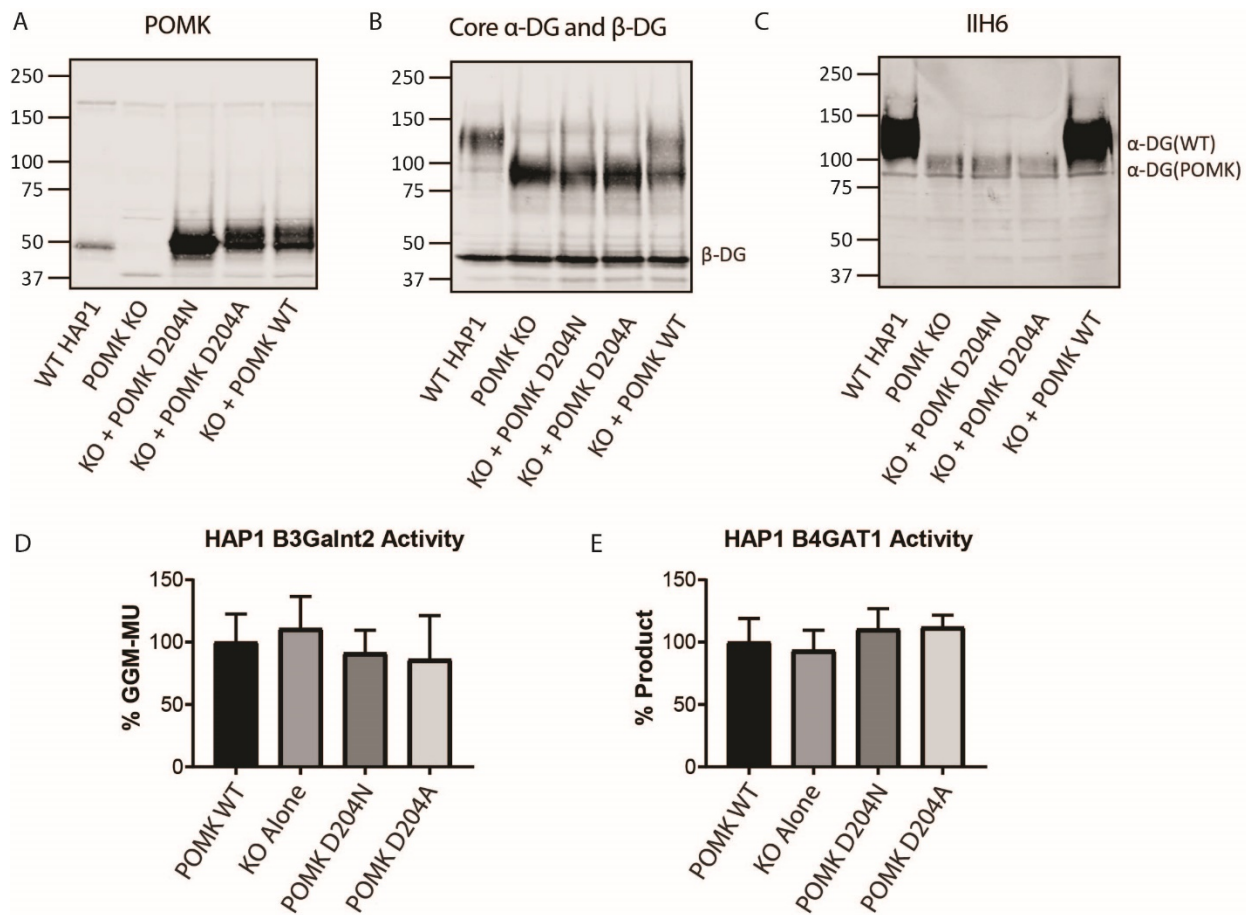
1217 **Figure 5 - Figure Supplement 1.** Solid-Phase Binding Analyses of POMK KO Skeletal Muscle.  
1218 **A**, Solid-phase binding analysis (relative  $B_{max}$  for laminin-111) of control, M-POMK KO (MCK-  
1219 Cre; Pax7-Cre; POMK<sup>LoxP/LoxP</sup>), MCK-Cre; POMK<sup>LoxP/LoxP</sup>, and *LARGE*<sup>myd</sup> skeletal muscle  
1220 (three replicates). Error bars: standard deviation. **B**, Solid-phase binding analysis of MCK-Cre;  
1221 POMK<sup>LoxP/LoxP</sup> skeletal muscle treated in combination with Xylsa and Bgus for 0 or 20 hours.  
1222 Results from three independent experiments are shown. Error bars: standard deviation.

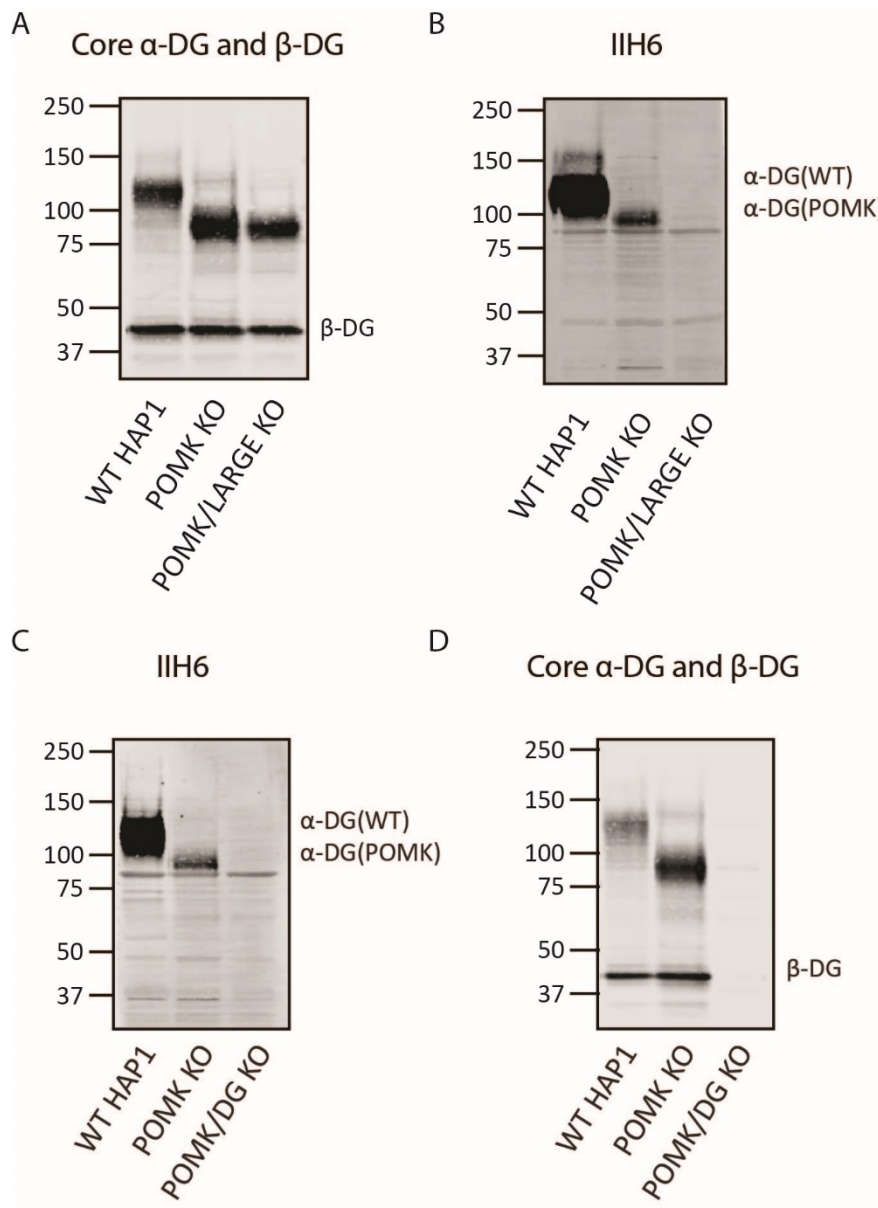
1223



1224

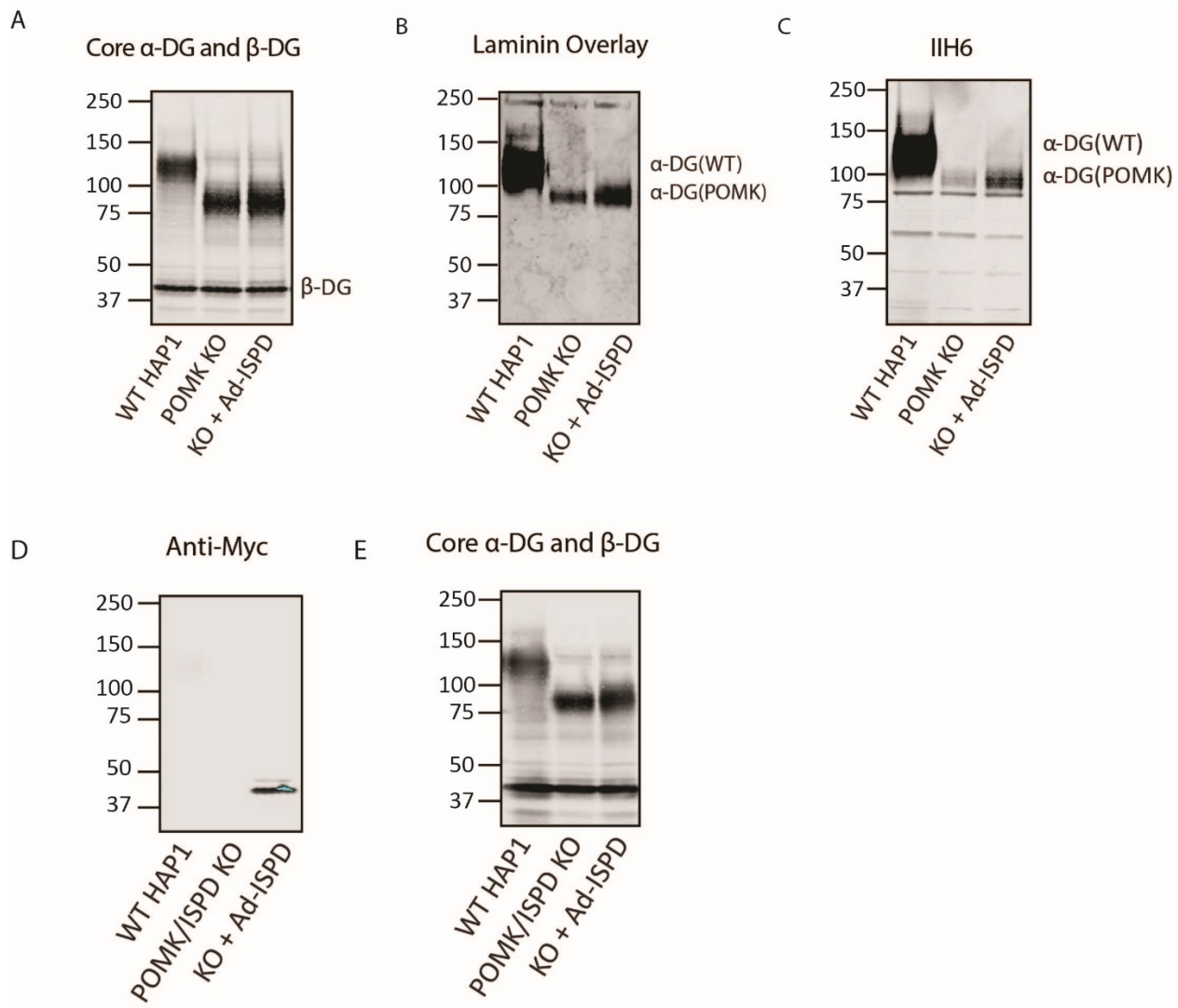
1225 **Figure 5 - Figure Supplement 2. POMK Knockout Muscle Expresses Matriglycan. A, B,**  
1226 Glycoproteins were enriched from skeletal muscles of M-POMK KO, control, and *LARGE*<sup>myd</sup>  
1227 mice and treated in combination with α-xylosidase (Xylsa) and β-glucuronidase (Bqus).  
1228 Immunoblotting was performed with **A**, AF6868 (core α-DG and β-DG) and **B**, IIH6  
1229 (matriglycan). Results from three independent experiments are shown. Asterisk: β-DG. **C**, A  
1230 laminin overlay was performed of control M-POMK KO skeletal muscle and heart.  
1231 Glycoproteins were enriched from heart as above (three replicates).



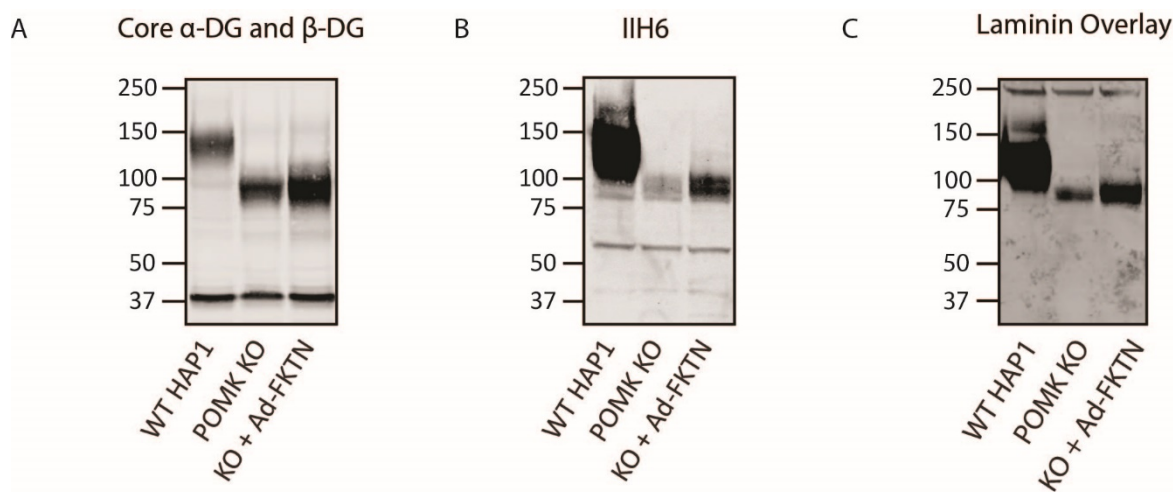


1242 **Figure 7 - Figure Supplement 1.** Supplemental Biochemical Analysis of *POMK/LARGE* KO  
1243 and *POMK/DG* KO HAP1 Cells. **A, B** Immunoblotting of WT, *POMK* KO and *POMK/LARGE*  
1244 KO HAP1 cells with antibodies AF6868 (**A**), Core  $\alpha$ -DG and  $\beta$ -DG) or IIH6 (**B**). Glycoproteins  
1245 were enriched using WGA-agarose as described in the Methods. **C, D** Immunoblotting of WT,  
1246 *POMK* KO, and *POMK/DG* KO HAP1 cells with antibodies IIH6 (**C**) or AF6868 (**D**, Core  $\alpha$ -DG  
1247 and  $\beta$ -DG). Representative results from three independent experiments are shown.

1248

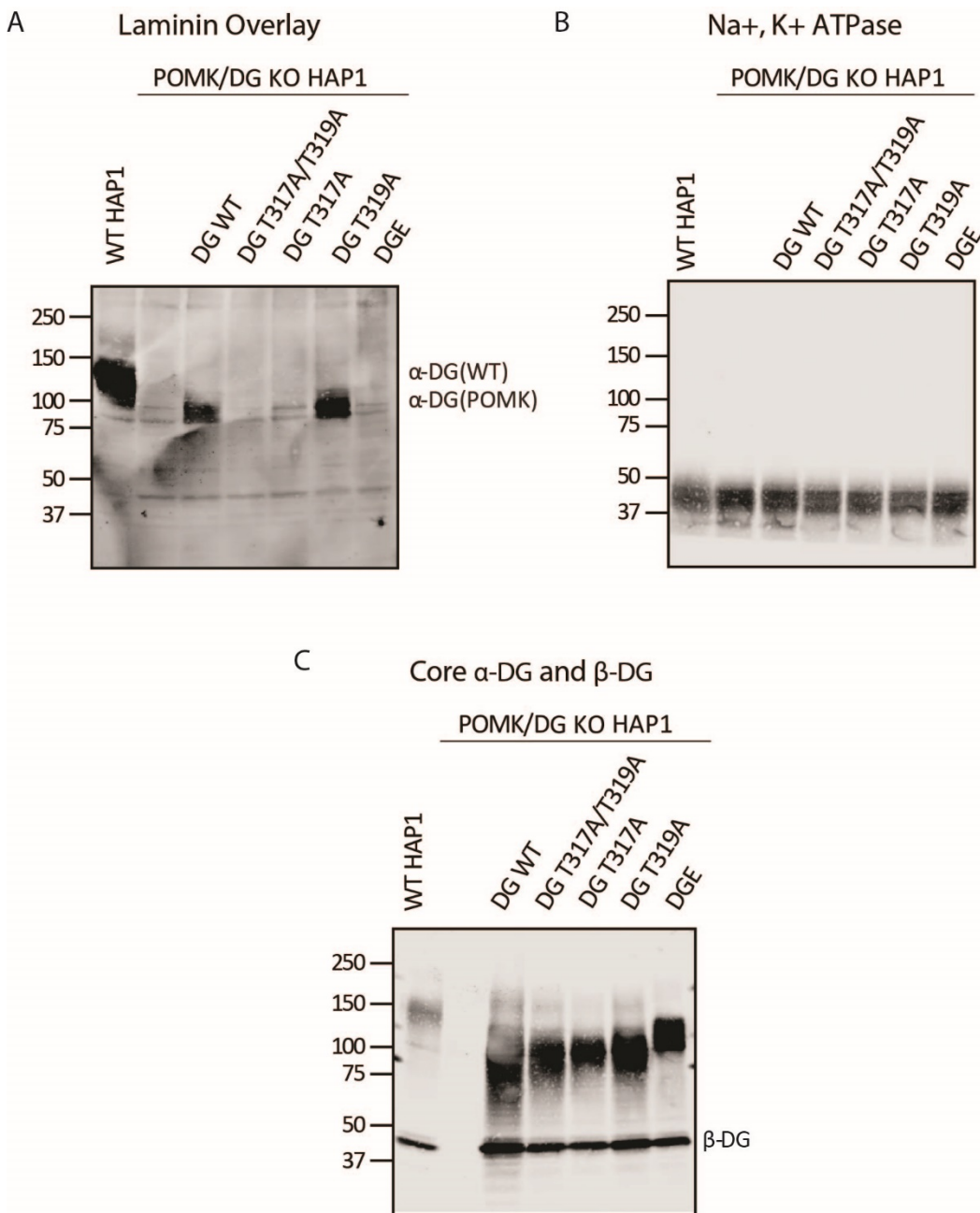


1250 **Figure 7 - Figure Supplement 2.** Requirement for Ribitol-Phosphate in the Synthesis of the  
1251 Non-Extended Matriglycan. **A, B, C,** *POMK* KO HAP1 cells were transduced with an  
1252 adenovirus encoding Isoprenoid Synthase Domain-Containing (Ad-ISPD). Immunoblotting was  
1253 performed using antibodies AF6868 (**A**) or IIH6 (**C**). **B**, A laminin overlay was also performed.  
1254 Representative results from three independent experiments are shown. **D, E**, HAP1 cells lacking  
1255 expression of ISPD and POMK (*POMK/ISPD* KO) were transduced with Ad-ISPD.  
1256 Immunoblotting was performed with an anti-Myc antibody (**D**) or antibody AF6868 (**E**, Core  $\alpha$ -  
1257 DG and  $\beta$ -DG). Representative results from three independent experiments are shown.



1258

1259 **Figure 7 - Figure Supplement 3.** Fukutin Overexpression Enhances Synthesis of the Non-  
1260 Extended Matriglycan. **A, B, C,** *POMK* KO HAP1 cells transduced with an adenovirus encoding  
1261 Fukutin (FKTN), Ad-FKTN. Immunoblotting was performed using antibodies AF6868 (**A**), Core  
1262 α-DG and β-DG) or IIH6 (**B**) (three replicates). **C**, A laminin overlay was also performed (three  
1263 replicates).



1264  
1265

1266 **Figure 7 - Figure Supplement 4.** T317 is Required for Synthesis of the Non-Extended  
1267 Matriglycan. **A, B, C** Biochemical analysis of *POMK/DG* KO HAP1 cells expressing the  
1268 indicated adenoviruses (three replicates). DGE is for viral expression of α-DG that lacks the  
1269 Dystroglycan N-terminal domain (DGN). **A**, A laminin overlay was performed. Immunoblotting  
1270 was performed with an Na<sup>+</sup>/K<sup>+</sup> ATPase antibody (**B**) and antibody AF6868 (**C**, Core α-DG and  
1271 β-DG).

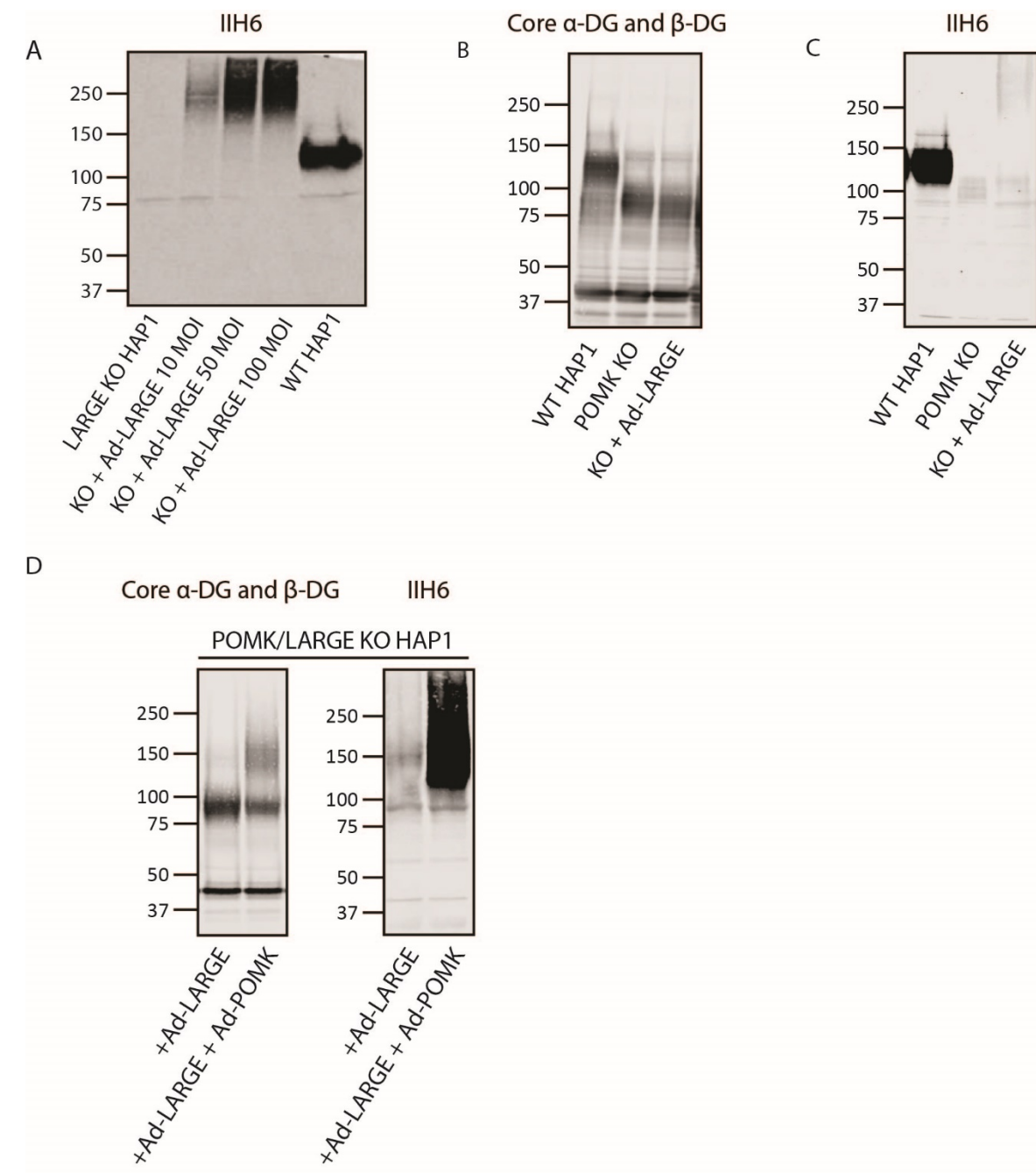
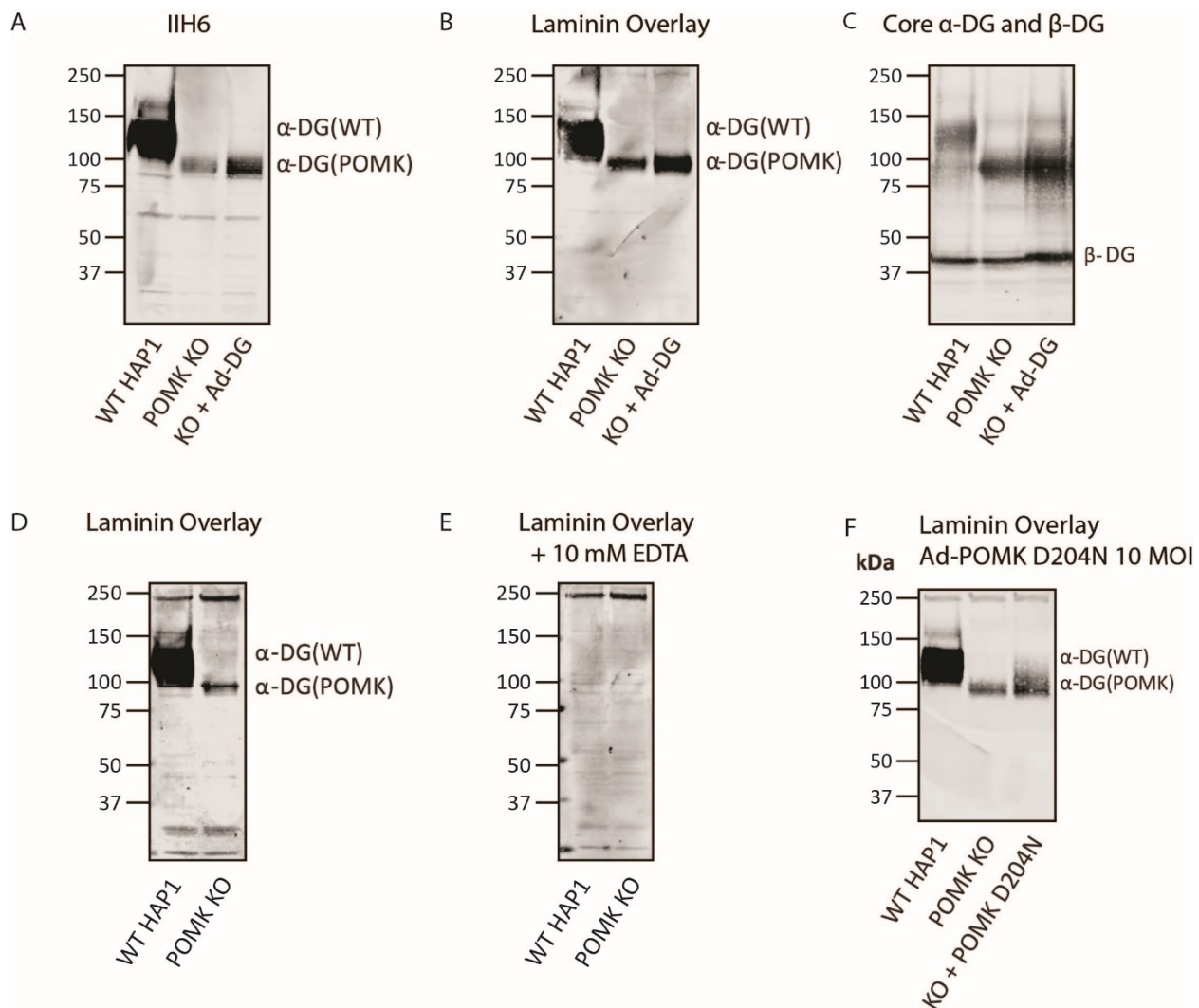


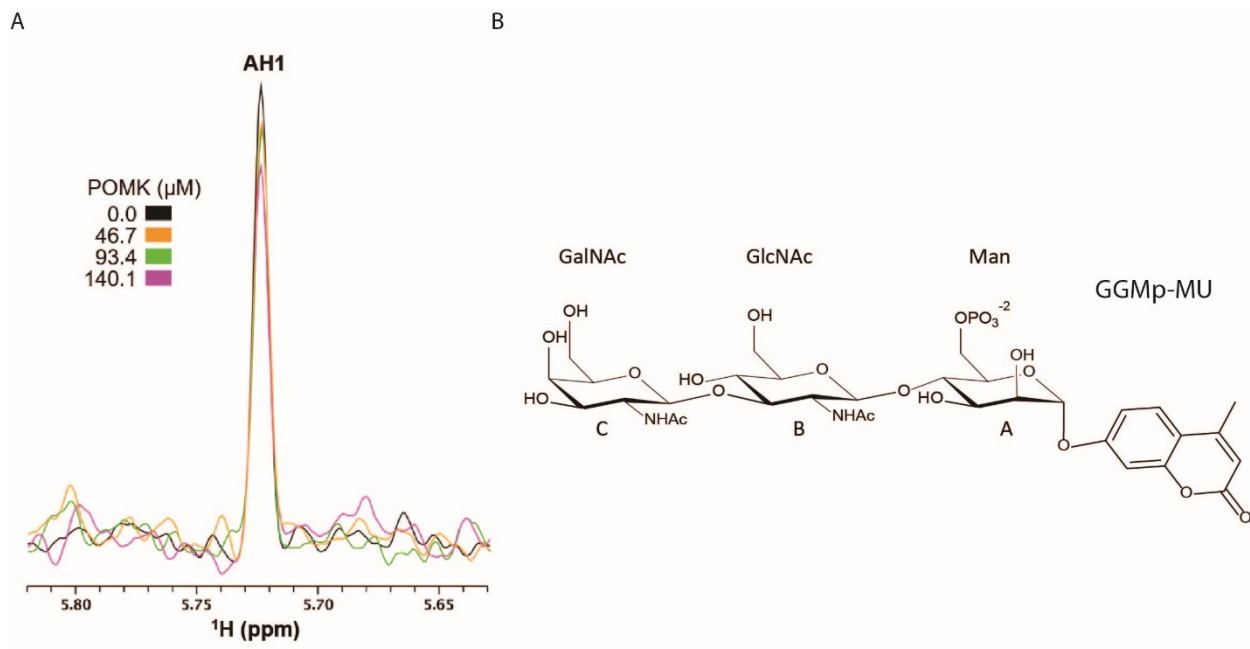
**Figure 7 - Figure Supplement 5.** POMK Enables LARGE-mediated Elongation of Matriglycan.  
**A, B, C,** Immunoblots of the following HAP1 cells: **A**, *LARGE* KO, overexpressing Ad-*LARGE*; **B, C**, *POMK* KO, overexpressing Ad-*LARGE*; **D**, *POMK/LARGE* KO, overexpressing Ad-*LARGE* with or without Ad-*POMK*. Immunoblotting was performed with antibodies AF6868 (Core  $\alpha$ -DG and  $\beta$ -DG) or IIH6 (three replicates).



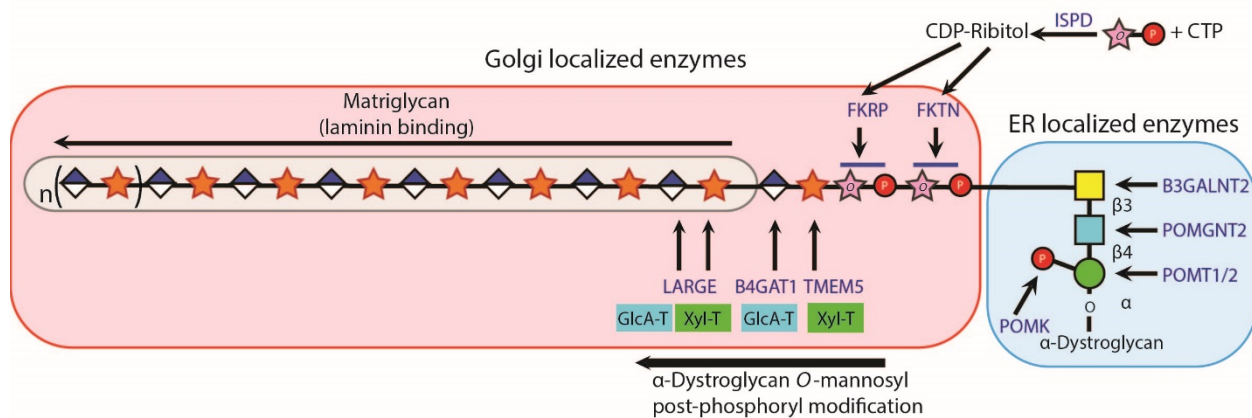
1279

1280

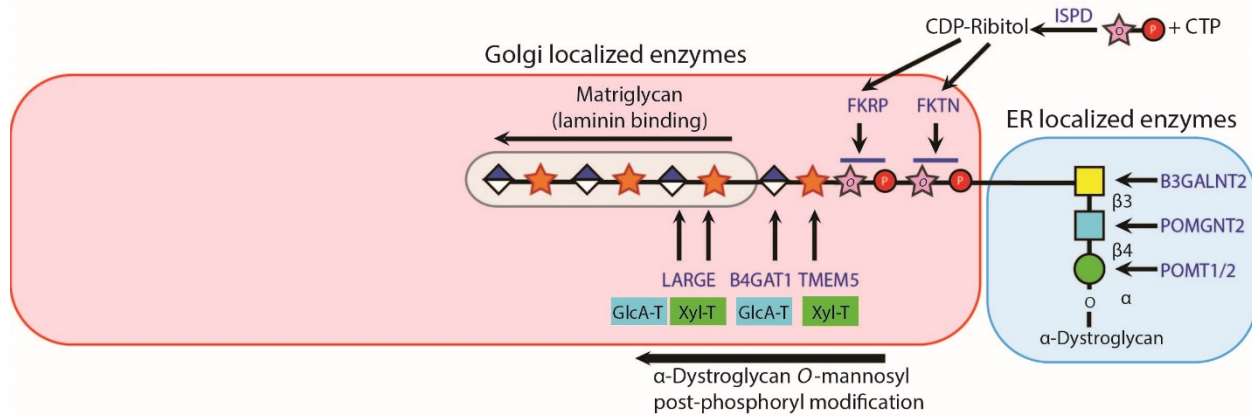
1281 **Figure 7 - Figure Supplement 6.** Supplemental Characterization of POMK-null Matriglycan  
1282 Synthesis. **A, B, C,** *POMK* KO HAP1 cells were transduced with an adenovirus encoding DG  
1283 (Ad-DG) and immunoblotting was performed with antibodies IIH6 (**A**) and AF6868 (**C**) (three  
1284 replicates). A laminin overlay was also performed (**B**) (three replicates). **D, E,** Laminin overlays  
1285 of WT and *POMK* KO HAP1 cells were performed without (**D**) or with (**E**) EDTA (three  
1286 replicates). **F,** A laminin overlay of WT HAP1, *POMK* KO HAP1, or *POMK* KO HAP1 cells  
1287 transduced with 10 MOI Ad-*POMK* D204N was performed (three replicates).



A



B



1296

1297 **Figure 8 - Figure Supplement 2.** Model of Full-Length and Non-extended Matriglycan  
1298 Synthesis. **A**, Mature matriglycan is a long polysaccharide that is synthesized by LARGE. **B**, In  
1299 the absence of the core M3 phosphate added by POMK, LARGE generates a shorter, non-  
1300 extended form of matriglycan.

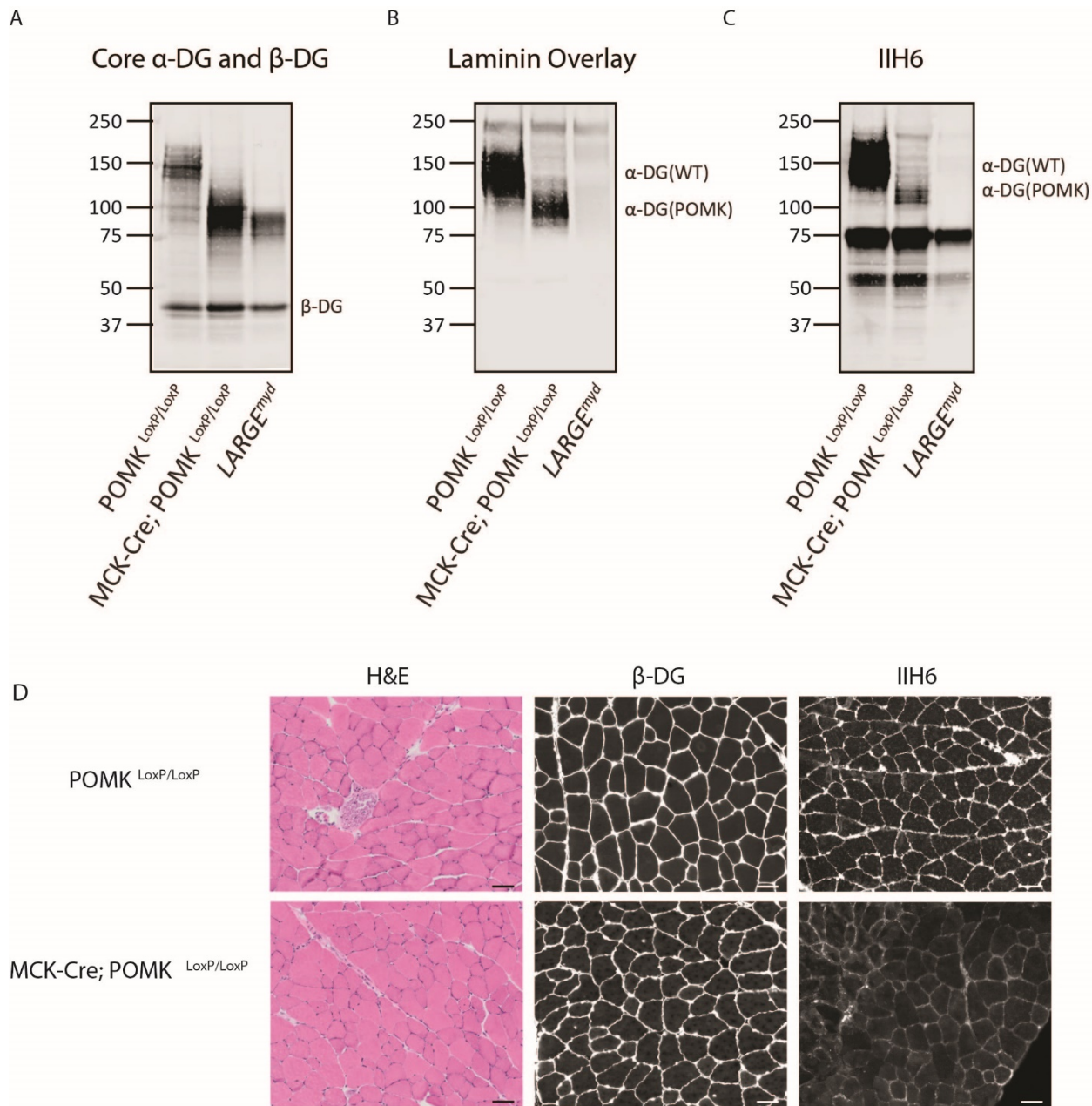
1301

1302

1303

1304

1305



1307 **Figure 8 - Figure Supplement 3.** Biochemical and Histologic Analysis of MCK-Cre;  
1308 POMK<sup>LoxP/LoxP</sup> Quadriceps Muscle. **A, B, C,** Representative biochemical analysis of  
1309 glycoproteins enriched from quadriceps skeletal muscles of POMK<sup>LoxP/LoxP</sup>, MCK-Cre;  
1310 POMK<sup>LoxP/LoxP</sup>, and LARGE<sup>myd</sup> mice using WGA-agarose (three replicates). For immunoblotting,  
1311 antibodies AF6868 (**A**) and IIH6 (**C**) were used, and a laminin overlay was also performed (**B**).  
1312 **D,** Immunofluorescence and H&E analyses of POMK<sup>LoxP/LoxP</sup> and MCK-Cre; POMK<sup>LoxP/LoxP</sup>  
1313 quadriceps muscle sections from 8-month old mice. Sections were stained with antibodies  
1314 against  $\beta$ -DG (middle) and matriglycan (IIH6) (right). Histologic abnormalities in the sections  
1315 were evaluated by means of hematoxylin and eosin (H&E) staining (left). Scale bars- 50  $\mu$ M  
1316 (three replicates).